



PES UNIVERSITY
(Established under Karnataka Act no. 16 of 2013)
100-ft Ring Road, Bengaluru - 560 085, Karnataka, India

Dissertation on

Target Classification Using Millimeter Waves

Submitted by

Aditya Suresh Prabhu (01FB14EEC010)
Debayan Ghosh (01FB14EEC055)

Jan. - Apr. 2018

under the guidance of

External Guide

Dr. Abhay Sharma
Member Technical Staff
Robert Bosch Centre for Cyber Physical Systems
Indian Institute of Science
Bengaluru - 560012

Internal Guide

Dr. Sanjeev G.
Professor
Department of Electronics and Communication Engineering
PES University
Bengaluru - 560085

FACULTY OF ENGINEERING
DEPARTMENT OF ELECTRONICS AND COMMUNICATION ENGINEERING
PROGRAM: BACHELOR OF TECHNOLOGY (ECE)



FACULTY OF ENGINEERING
DEPARTMENT OF ELECTRONICS AND COMMUNICATION ENGINEERING
PROGRAM: BACHELOR OF TECHNOLOGY (ECE)

CERTIFICATE

This is to certify that the dissertation entitled

Target Classification Using Millimeter Waves

is a bona fide work carried out by

Aditya Suresh Prabhu (01FB14EEC010)

and

Debayan Ghosh (01FB14EEC055)

In partial fulfillment for the completion of 8th semester course work in the Program of Study B.Tech in Electronics and Communication Engineering under rules and regulations of PES University, Bengaluru during the period Jan. 2018 - Apr. 2018. It is certified that all corrections/suggestions indicated for internal assessment have been incorporated in the report. The dissertation has been approved as it satisfies the 8th semester academic requirements in respect of project work.

Signature with date & seal Signature with date & seal Signature with date & seal
Internal guide Chairperson Dean of Faculty

DECLARATION

We, Aditya Suresh Prabhu and Debayan Ghosh, hereby declare that the dissertation titled, ***“Target Classification Using Millimeter Waves”***, is an original work done by us under the guidance of Dr. Abhay Sharma, Member Technical Staff, Robert Bosch Centre for Cyber Physical Systems, Indian Institute of Science, and Dr. Sanjeev G., Professor, Department of Electronics and Communications Engineering, PES University, and is being submitted in partial fulfillment of requirements for the completion of 8th semester coursework in the Program of Study B.Tech in Electronics and Communication Engineering.

PLACE:

DATE:

NAME AND SIGNATURE OF THE CANDIDATES:

Aditya Suresh Prabhu

Debayan Ghosh

Acknowledgement

We would like to express our gratitude to our guides Dr. Abhay Sharma and Dr. Sanjeev G., without whose guidance this project would not have been possible. They have encouraged us to delve deeper into the subject ensuring we enjoy the overall experience. We thank Dr. Ganesan Thiagarajan for his insightful inputs and suggestions. We express our gratitude to members of the project review panel for their insights and suggestions. Our heartfelt thanks to our chairpersons over the past four years, Dr. Anuradha M. and Dr. T. S. Chandar for creating an environment conducive to learning, helping us appreciate our coursework better. We thank the Vice-Chancellor and other members of management of PES University for inspiring and encouraging us to be better individuals.

We thank Chirag Ramesh, Rakshit Ramesh, Preetham Hegde and all our lab mates at the Robert Bosch Centre for Cyber Physical systems for their help, support and engaging conversations over coffee. Our friends and classmates have played a huge role in shaping our outlook and belief, and we thank each and every one of them. We thank our teachers for encouraging us to give our best, and inspiring us to think differently. We have spent four fruitful years at PES University, and we thank each and every member of PES University for making this time enjoyable. Last but not least, we thank our parents for supporting us and believing in us through all these years.

Abstract

Radar systems have been under development since the early twentieth century. Over the past few decades, significant progress has been made in the field, including the development of radars operating in the *millimeter wave* range of frequencies between 30 GHz to 300 GHz. The millimeter wave radars have found applications in areas such as gesture recognition and vehicle autonomy. In this dissertation, we investigate the use of these millimeter wave radars in classifying the targets detected. The fine range and velocity resolutions provided by the radar are exploited to study the motion of targets using micro-doppler analysis. In particular, we use the AWR1642 FMCW radar sensor developed by the Texas Instruments to collect and analyze data.

Simple simulation models are developed to study the performance of the relevant signal processing algorithms, under different operating conditions. The results obtained from these simulations and from those proposed earlier in the literature are used to develop different setups to collect data, and study them. Two feature extraction schemes are discussed, which are used to train three types of classifiers, namely, the Naïve Bayes' classifier, support vector machine, and the K-nearest neighbor classifier. The ability to distinguish between the rotating and non-rotating targets is demonstrated with an accuracy of upto 90%, when the classifiers are trained individually using each feature extraction method.

List of Figures

2.1	Different profiles for frequency variation	4
4.1	A simple block diagram of an FMCW radar system	10
4.2	A chirp signal in time domain	12
4.3	Frequency time plot depicting the transmitted and received signals	12
4.4	Transmitted, received and mixed signals outputs	13
4.5	Transmitted, received and mixed signal outputs for multiple targets	14
4.6	An illustration of the steps required to obtain the range-doppler profile	17
4.7	3-D radar data cube with FFT of AoA evaluation shown	18
4.8	Frequency - time plot showing chirp time T_c , idle time T_i and pulse time T_r .	19
5.1	Range-doppler profile for a target located at 10m with a velocity of 10m/s .	21
5.2	Range-Doppler profile of a target outside the maximum detectable range .	21
5.3	Range-doppler profile for two targets at 5m and 8m, moving with velocities 10m/s and 20m/s	22
5.4	Range-doppler profile for two targets at 5m and 5.5m, moving with a ve- locity of 10m/s	23
5.5	Range-doppler profile for two targets at 5m and 5.5m, moving with veloci- ties 10m/s and 20m/s	23
5.6	Range-doppler profile for two targets at 15m and 20m, moving with velocity 20m/s	24
5.7	Range-doppler profile for two targets at 30m, moving with velocity 20m/s and 22m/s	24
5.8	Proposed point cloud model	25
5.9	Point Cloud Model: Contour, mesh and range plot for a single target at 4m and 0° azimuth	27
5.10	Point Cloud Model: Contour, mesh and range plot for a single target at 4m and -10°	28
5.11	Point Cloud Model: Contour, mesh and range plot for a multiple targets at 3m, 5m, 7m and 0° azimuth	29
5.12	Point Cloud Model: Contour, mesh and range plot for a multiple targets at 3m, 5m, 7m, with azimuth angles of -10° , 0° , 10° respectively	30

5.13 Point Cloud Model: Contour, mesh and range plot for a multiple targets of area 0.2 sq.m, at 3m, 5m, 7m, with azimuth angles of -10° , 0° , 10° respectively	31
6.1 Simple diagram of rotor blade to illustrate change in doppler frequency	33
6.2 Short-Term Fourier Transform spectrum of rotating objects	34
6.3 STFT of an accelerating target	34
6.4 Challenges in extracting micro-doppler information	35
7.1 The TI-AWR1642 mmWave radar	37
7.2 Sample configuration file with each field labelled	38
7.3 A schematic of sensor with L3 memory and communication ports highlighted	39
7.4 A view of the environment for first round of data collection	40
7.5 Range profile of two consecutive frames in dataset-1	41
7.6 A view of the environment for the second round of data collection	42
7.7 Range-doppler profile for dataset-2	43
7.8 A view of the environment for the second round of data collection	44
7.9 Range profile for the target kept at 2m	45
7.10 Range-doppler profile for the target kept at 2m	46
7.11 Micro-doppler profile for different objects	47
7.12 Micro-doppler profile for a fan: rotating v/s stationary	49
7.13 Micro-doppler signature for reflector with (a) rotational velocity (b) translational velocity. Notice the sinusoidal behaviour for the rotational case	49
7.14 Steps in correlation method - rotating object	51
7.15 Steps in correlation method - object with linear velocity	52
7.16 Steps in correlation method - object with linear velocity	52
7.17 Fourier Transform v/s Mean Frequency Profile	53
7.18 Mean Frequency Profile for different kinds of motion	54
A.1 Diagram to derive relationship between target velocity and doppler frequency	59
A.2 Diagram to derive doppler frequency for object not moving along line of sight	60
B.1 STFT for the test signal	63
B.2 WVD for the test signal	63
B.3 PWVD for the test signal	63
B.4 WVD masked with STFT	64

List of Tables

7.1	Configuration parameters for round-1 of data collection	41
7.2	Configuration parameters for round-2 of data collection	43
7.3	Configuration parameters for round-3 of data collection	45
7.4	Configuration parameters for round-4 of data collection	48
7.5	Confusion matrix for the Naïve Bayes classifier using the correlation method for feature extraction	55
7.6	Confusion matrix for the SVM classifier using the correlation method for feature extraction	55
7.7	Confusion matrix for the KNN classifier using the correlation method for feature extraction	55
7.8	Overall accuracy for the classifiers using the correlation method for feature extraction	55
7.9	Confusion matrix for the Naïve Bayes classifier using the PCA method for feature extraction	56
7.10	Confusion matrix for the SVM classifier using the PCA method for feature extraction	56
7.11	Confusion matrix for the KNN classifier using PCA method for feature extraction	56
7.12	Overall accuracy of classifiers using the PCA method for feature extraction	56

Contents

Acknowledgments	i
Abstract	ii
1 Introduction	1
1.1 Motivation and Problem Formulation	1
1.2 Organization of Dissertation	2
2 Background	3
2.1 Radar and Its Types	3
2.1.1 Pulsed radar	3
2.1.2 Unmodulated Continuous Wave (UCW) radar	4
2.1.3 Frequency Modulated Continuous Wave (FMCW) Radar	4
2.2 Radar Resolution Parameters	4
2.3 Radar Range Equation	5
2.4 Millimeter Wave Radar	6
3 Related Work	7
4 Frequency Modulated Continuous Wave Radar	10
4.1 Transmit and Receive Signal Models	10
4.2 Measuring Range and Velocity	13
4.2.1 Evaluating Range	13
4.2.2 Evaluating Velocity	15
4.2.3 Algorithm To Evaluate Range-Doppler Profile	16
4.3 Measurement of Angle of Arrival	17
4.4 Chirp Design	18
5 Simulation Models	20
5.1 Simple Target Model	20
5.1.1 Single Target	20
5.1.2 Two targets	22
5.2 Point Cloud Model	25

5.2.1	Single Target	26
5.2.2	Multiple Targets	28
6	Analysis of Micro-Motion	32
6.1	Micro-Motion and The Doppler Effect	32
6.2	Micro-Doppler Analysis	33
7	Data Collection and Classification	37
7.1	The TI-AWR1642 Millimeter Wave Radar	37
7.1.1	Controlling Sensor Operation	38
7.1.2	Data Extraction	38
7.2	Data Visualisation	40
7.2.1	Dataset - I	40
7.2.2	Dataset - II	42
7.2.3	Dataset - III	44
7.2.4	Dataset - IV	48
7.3	Feature Extraction	50
7.3.1	Correlation Method	50
7.3.2	Principal Component Analysis Method	53
7.4	Classification	54
7.4.1	Classification Using the Correlation Method	54
7.4.2	Classification Using the PCA Method	55
8	Conclusion and Future Work	58
Appendices		58
A	Doppler Effect	59
B	Time-Frequency Distributions	61
B.1	Short Term Fourier Transform (STFT)	61
B.2	Wigner-Ville Distribution (WVD)	62
B.3	Pseudo-Wigner Ville Distribution (PWVD)	62
Bibliography		66

Chapter 1

Introduction

The development of radar systems as we know it today began during the early days of World War II [1]. At the time, the need for these systems was to identify enemy aircraft. Today, the fundamental ideas used in such systems have been borrowed by other technologies such as Radio Frequency Identification (RFID) [2], and found applications in areas such as autonomous driving and gesture recognition [3, 4]. The objective of our dissertation however, is to investigate the use of radars in the identification and classification of targets within its field of view. In the subsequent sections, we present our problem statement, along with some motivation to appreciate the need to solve the same.

1.1 Motivation and Problem Formulation

In these past few years, India and other countries have been moving towards building *smart cities*. A few major components of this exercise include smart surveillance techniques, smart delivery systems and so on. Unmanned Aerial vehicles (UAVs) or drones are expected to be important in realising these goals. A key issue with using UAVs, is to ensure they stay in a designated corridor, and do not intrude into other areas. This requires us to monitor a given environment, and ensure there is no intrusion. This monitoring could be implemented using video surveillance, or sensors such as the Kinect [5, 6], but since it uses image-sensing to recognise objects (targets), it could be intrusive and infringe upon the privacy of citizens. Using a radar based sensor might help us achieve our aim of monitoring a given environment, while addressing privacy concerns. This larger problem can be broken down into multiple smaller sub-problems, one of which is to develop a scheme to identify distinguishing features between various possible targets.

We focus on attempting to identify targets with components displaying periodic motion (for example, rotation) and find what characteristics distinguish them from objects without such a motion. We then implement classification algorithms to distinguish between targets based on these observed features. We use a Frequency Modulated Continuous Wave (FMCW) radar operating in the 76 GHz - 81 GHz range of frequencies, developed by Texas

Instruments as our sensor [7]. The advantage of using this range of frequencies, are the fine range and velocity resolutions that can be obtained. These points are discussed in greater detail in the further chapters. Thus, having developed some appreciation towards the relevance of the problem we formally state it as follows

Given a Frequency Modulated Continuous Wave millimeter wave radar sensor, develop a signal processing and classification scheme to detect and identify whether a target in its field of view is one with rotating parts or not.

1.2 Organization of Dissertation

The organisation of the remainder of this dissertation is as follows. Chapter 2 is a review of the radar fundamentals, and has definitions of a few terms used in this dissertation. A literature survey is presented in Chapter 3. The operation of a Frequency Modulated Continuous Wave radar is discussed in chapter 4, some of which is incorporated into developing simulation models used in chapter 5. Chapter 6 discusses micro-motion analysis, used to obtain insight into the nature of an objects motion over time.

The theoretical knowledge obtained from these chapters, is validated on data collected in chapter 7. A simple binary classification problem is also solved in this chapter, distinguishing between rotating and non-rotating targets. The conclusion and work to be done in the future is presented in chapter 8, with the bibliography consisting of the references concluding the dissertation.

Chapter 2

Background

In this chapter, we introduce the terms and definitions used in this dissertation. Textbooks on antenna theory and radar systems [8, 9], and radar systems are referred to develop a better understanding of the subject.

2.1 Radar and Its Types

A Radar is a system used to detect, and localise objects in space. An object can be localised, by evaluating its distance, velocity and angular position relative to the radar. In radar literature, an object is also referred to as a *target*. A radar achieves this function, by transmitting an electromagnetic signal and analysing the received echo, after reflections from objects within its field of view. Depending on the type of signals used to look for objects, we can classify radars into the following types

- Pulsed radar
- Unmodulated Continuous Wave (UCW) radar
- Frequency Modulated Continuous Wave (FMCW) radar

We now examine each of these types, and understand the advantages and limitations of each.

2.1.1 Pulsed radar

In this type of radar, the transmitter is switched on for a very short duration time, following which the receiver is switched on to listen for the echo. This echo signal indicates the presence of a target as well as the distance to the target by measuring the time delay between the transmitted signal and echo. The important point to note here, is that transmitted and received signals are separated only in time, which means it is not possible to measure velocity using this scheme.

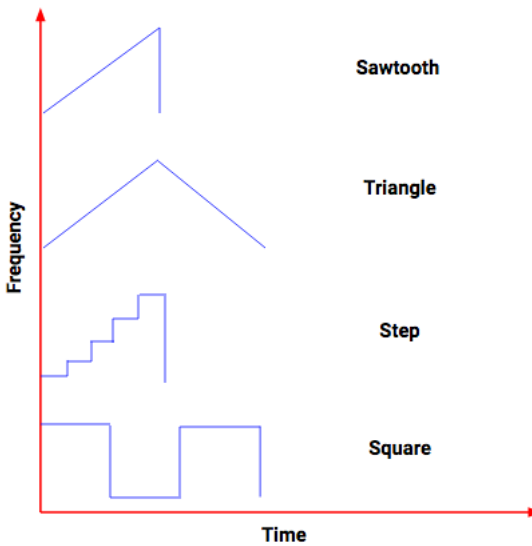


Figure 2.1: Different profiles for frequency variation

2.1.2 Unmodulated Continuous Wave (UCW) radar

In this type of radar, a continuous wave of known stable frequency is transmitted, and received after reflection from targets. It is not possible to determine the range as there is no isolation of any kind in time. However, this radar exploits the phenomenon of doppler shift to evaluate the velocity of a moving target [10].

2.1.3 Frequency Modulated Continuous Wave (FMCW) Radar

The UCW radar has a limitation in that it cannot be used for range estimation as it operates at one stable frequency. FMCW radars help us overcome this limitation, by being able to change operating frequency during the window of measurement. This is achieved by the use of frequency modulation. There are different profiles which can be followed while varying the operating frequency. Some of these include: linear or sawtooth, triangle, step and square. Figure 2.1 illustrates these profiles.

Upon listing the advantages and disadvantages of each of these above classes, it is somewhat clear that FMCW radars are well suited to our application, as they localise targets in both range and velocity. In the next section, we look at two radar parameters, namely the range and velocity resolutions.

2.2 Radar Resolution Parameters

In the previous section, range, velocity and angular position were listed to be three variables a radar evaluates to localise a target. We now ask the following question: *What is the closest that two targets can be in range, velocity, and angular position and still be uniquely*

identified? It is the answer to this question, that leads us to the definitions of range, velocity and angle resolution, which are as follows

- Range resolution: It is defined to be smallest distance of separation between two targets, which enables their unique identification by a radar.
- Velocity resolution: It is defined to be the minimum separation between the velocities for it to be uniquely identified by a radar.
- Angle resolution: It is defined to be the minimum angular separation between the positions of two objects, for them to be uniquely detected by a radar.

Having understood some of these parameters, we now study the radar range equation and radar cross sections of targets, which are used to characterise the medium of transmission and targets in that medium respectively.

2.3 Radar Range Equation

In this section, we begin by defining the Radar Cross Section of a target as given by Balanis [8]. Let us assume a certain amount of transmitted power is incident upon a target. Then, the radar cross section is defined as *the area intercepting that amount of power, which when scattered uniformly in all directions, produces at the receiver a density which is equal to that scattered by the actual target*. This is mathematically represented as

$$\sigma = \lim_{R \rightarrow \infty} \left[4\pi R^2 \frac{W_s}{W_i} \right] \quad (2.1)$$

where

σ = radar cross section (m^2)

R = range of the target (m)

W_i = incident power density (W/m^2)

W_s = scattered power density (W/m^2)

The radar range equation, describes a relationship between the power levels of the transmitted and received signals in a radar. Assuming the transmit and receive antennas are polarisation matched, of ideal efficiency, and are located at the same distance from the target, we can mathematically write it as

$$\frac{P_r}{P_t} = \sigma \frac{G_t G_r}{4\pi} \left[\frac{\lambda}{4\pi R^2} \right]^2 \quad (2.2)$$

We see that the received power is directly proportional to the radar cross section σ given by equation 2.1 and inversely proportional to the square of the distance between the antenna and target, or the range of the target.

2.4 Millimeter Wave Radar

A millimeter wave radar is one that operates in the range of frequencies between 30GHz to 300Hz, with the wavelength of the order of 10^{-3} m. There are both advantages and limitations while operating in the millimeter range of frequencies, as we shall see in further chapters. The main advantage is that it offers good range and velocity resolutions. The disadvantage, is that such waves are more prone to interference, consequently limiting the maximum range which can be detected.

Thus far, we have understood the basics concepts of a radar, and looked at a few terms and their definitions. In the next chapter, discuss some of the work done in this area until today.

Chapter 3

Related Work

The fundamentals of antenna theory are discussed in the textbook written by Balanis [8]. In this book, elementary concepts such as directivity and beamwidth are discussed, along with discussions on the types of antennas such as wire antennas, loop antennas, and antenna arrays. An understanding of such fundamental concepts is essential to appreciate the capabilities provided by Texas Instrument's AWR1642 millimeter wave radar sensor used in this project. An introduction to radar systems is available in the textbook by Skolnik [9]. The book introduces us to different types of radar systems, and the radar range equation.

We use a Frequency Modulated Continuous Wave (FMCW) radar for our application. The paper by Barrick [11] provides mathematical insight into the signal processing scheme required to analyze data generated using FMCW radars. Sandeep Rao's lecture series [12] discusses signal processing using FMCW radars in the context of millimeter wave signals, along with the relevant tradeoffs in system and hardware design. The concepts discussed in the above sources are essential in forming a big picture of the system required to realise the goals of this project.

The elementary signal processing operations described by the literature reviewed thus far does not provide sufficient information about a target's motion. In order to study the finer aspects of a target's motion we need micro-doppler analysis. A paper by Suresh et al. [13] identifies time-frequency analysis along with techniques such as the Fractional Fourier Transform (FrFT) and Fourier-Bessel Transform (FBT) as the tool required to perform micro-doppler analysis. The textbook on time-frequency analysis by Cohen [14] provides in depth coverage of the various time-frequency analysis techniques that are required for our use.

In this project, target classification is treated as a machine learning problem. Thus, an understanding of machine learning algorithms is essential. Fundamental concepts in pattern classification and machine learning are covered in textbooks by Duda, and Bishop [15, 16]. The topics reviewed from these textbooks include Bayesian classification, Support vector Machines (SVM), and K-Nearest Neighbours algorithms. Concepts in probability theory

and linear algebra are also reinforced by referring to the chapters in these books. All of the classification algorithms we use require a training phase. This training is done using certain features extracted from datasets. Principal Component Analysis (PCA) is one step used in extracting such features, and is understood from the paper by Shlens [17].

The radar sensor used to collect real-world data is the AWR1642 developed by Texas Instruments [7]. This is an automotive radar operating in the frequency range of 76GHz to 81GHz, used at a centre frequency of 77GHz. A detailed procedure to operate this radar is available in the user guide [18]. This sensor uses complex baseband architecture [19]. The advantage of this architecture is that we can sample signals at the maximum frequency occurring in the data rather than having to sample at twice this maximum frequency. The datasets collected using this sensor are used to distinguish between rotating and non-rotating targets.

Millimeter wave sensing has been studied by both academia and industry, with some interesting applications being proposed. Project Soli by google ATAP [4] uses millimeter wave radars for gesture identification. The radar operates at a frequency of 60GHz, illuminating the human hand with a single beam. High temporal resolution of the radar is exploited to differentiate between different gestures. The human hand is modelled to be a cloud of discrete points which scatter an incident signal from the radar. The received signal is a superposition of the scattered signal from each of these points in the point cloud. A random forest classifier is used for the purpose of gesture classification. Data is collected by making multiple individuals perform a finite set of gestures such as the rotation of a knob, or flicking of a switch. The classifier is trained by extracting features from these datasets. The features extracted include conventional radar parameters such as the range and velocity, and novel features such as the velocity centroid. Apart from the signal processing and gesture classification pipeline, the authors also present a detailed picture of the system and hardware architecture of the sensor, including the Radio Frequency (RF) front end. Third party developers are allowed to build applications using this sensor, and an Application Programming Interface (API) is provided for this purpose. Wei and Zhang study the feasibility of using millimeter wave radios to track passive objects [20]. In their system called mTrack, a single transmitter along with two receivers placed in orthogonal planes are used to track the movement of an object. Specifically, an ability to track a pen with low error is demonstrated in this work. While the system seems to be elegant, it is constrained in having to place the received antennas along two orthogonal planes.

A detailed discussion on the micro-doppler effect in radars is found in the textbook by Chen [21]. Mathematical models of the received signal from targets having different geometries are outlined in this book. One such model for the received signal from a rotor of a helicopter is used to study aerial target classification by Rehman et al. [22]. This paper identifies micro-doppler analysis as a method to distinguish between aerial targets such as birds and Unmanned Aerial Vehicles (UAVs). The paper presents simulation results

at a frequency of 94GHz. Upon examining these results, one can conclude that there is a distinction between different types of aerial targets. Further insight into this problem is given by Molchanov in his PhD thesis [23]. Here, the author discusses different classes of motion and their associated micro-doppler signatures. Real world data is collected by using an X-band radar operating at 9.4GHz. Novel feature extraction schemes are proposed, the output of which is used to train classifiers such as the Naïve Bayes and the Support Vector Machine (SVM). Classification accuracies of upto 94% are obtained for the problem of aerial target classification. Another approach discussed by Zabalza et al. [24] finds the time average of the micro-doppler spectrum and uses this as a feature to train a classifier.

An alternative approach to feature extraction is discussed by Wit et al. [25]. Here, rather than deriving the micro-doppler spectrum the classification is done by mapping the range and velocity of a target alone. The paper specifically addresses the identification of a helicopter from its rotor blades. In this approach, the target is first localised in range and velocity by plotting a range-doppler profile. This is now treated as a matrix, whose dimensionality is reduced using Principal Component Analysis. The dimensionally reduced data is used to train a K-Nearest Neighbours algorithm to perform classification. However, the data used to train and test the classifier is generated through simulation and has not been validated on real-world datasets.

The ideas presented in the above literature are put together to come up with a signal processing and classification pipeline required to distinguish between rotating and non-rotating targets.

Chapter 4

Frequency Modulated Continuous Wave Radar

In this chapter, we understand the basic operation of an FMCW radar, a simple block diagram of which is given in figure 4.1. We will begin by studying the transmit and receive signal models, followed by an overview of the signal processing techniques required to analyze these signals. We will be combining explanations from Barrick [11] and Rao [12] during the course of our discussion, and the reader is encouraged to refer to their works for a deeper understanding of the topic.

4.1 Transmit and Receive Signal Models

In this section, we analyze the transmitted and received signals. Let us consider a signal of 100% duty cycle with a linear, upward frequency sweep (rising sawtooth) repeating every T_r seconds, with a sweep bandwidth B . We can also refer to the repetition time T_r as the chirp time T_c . In the event of our signal not having a 100% duty cycle, T_c is a fraction of T_r . That is, T_c is the actual time for which the frequency sweep is active. The signal can be

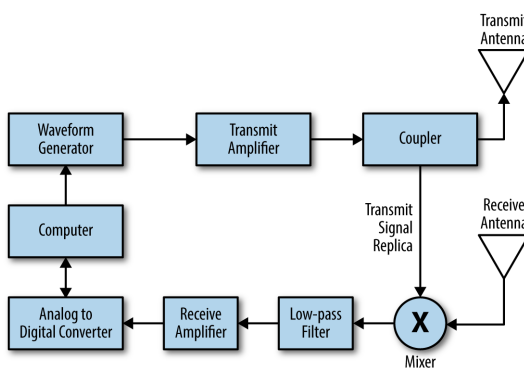


Figure 4.1: A simple block diagram of an FMCW radar system

mathematically written as

$$v_T(t) = \cos[\omega_c t + \pi B f_r t^2] \quad -\frac{T_r}{2} < t < \frac{T_r}{2} \quad (4.1)$$

where $f_r = 1/T_r$ is the pulse repetition frequency. Figure 4.2 shows a chirp signal in time domain obeying the above equation. The term in the argument of the cosine function can be written as $\phi_T(t)$. Let us assume a target is initially at some range R_0 and is moving with a velocity v . Thus, range of a target at a given instant of time can be expressed as a function of its velocity, given by

$$R = R_0 + vt \quad (4.2)$$

Upon analyzing the signal reflected off such a target, we can make the following observations

1. The signal is attenuated and delayed in time, which is dependant on the present range of the target.
2. There is a doppler shift in the received frequencies, due to relative motion between the target and the radar. Readers not familiar with the doppler effect and its relationship with the velocity can refer to appendix A.

Thus, the received signal can be mathematically represented as

$$v_R(t) = A v_T(t - \tau) = A \cos[\omega_c(t - \tau) + \pi B f_r(t - \tau)^2] \quad (4.3)$$

where time delay

$$\tau = \frac{2R}{C} \quad (4.4)$$

C being the speed of light.

A diagrammatic representation of the transmit and receive signal model is given in figure 4.3. In the figure, solid lines represent the transmit signals while the dotted lines represent the received signal. The time delay $\tau = 2R/C$ is shown in the figure. Notice how there is a slight difference in the frequency levels of the two signals. This is the shift caused by the doppler frequency, which is negative in this case (not labelled in the figure). Now, the received signal is applied to a mixer where it is multiplied with a copy of the transmitted signal, and passed through a low pass filter to remove high frequency components. This leaves us with an Intermediate Frequency (IF) signal given by

$$v_1(t) = A P_T(t) \cos[\omega_c(t - \tau) - \omega_c t + \pi B f_r(t - \tau)^2 - \pi B f_r t^2] \quad (4.5)$$

where $P_T(t)$ denotes a pulse of unity amplitude, and duration $T = T_r - \tau$. This term appears, as that is the only duration in time where both transmit and receive signals exist. Consider the first pair of transmit and received chirps. Assuming that the time delay τ is negligible

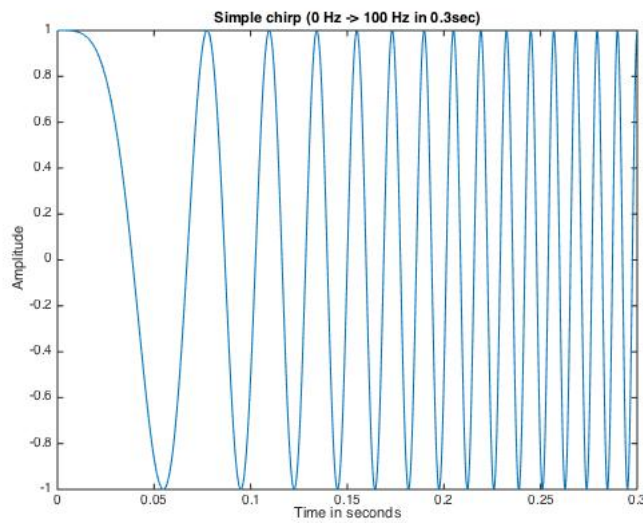


Figure 4.2: A chirp signal in time domain

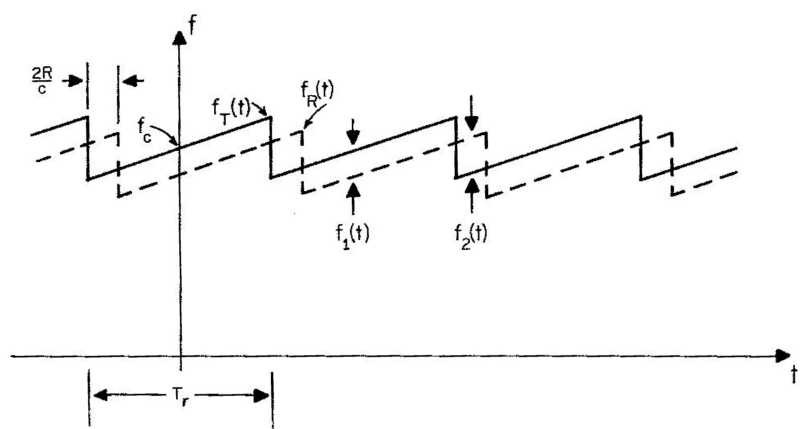


Figure 4.3: Frequency time plot depicting the transmitted and received signals. Received signal is in dotted lines. Source: D. E Barrick "FM/CW signals and digital processing", NOAA Tech.Report.ERL283-WPL,Tech.Rep.,1973

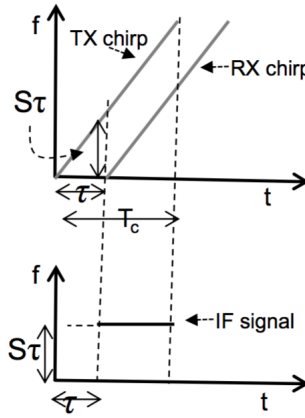


Figure 4.4: Transmitted, received and mixed signals outputs

compared to the chirp time T_r , simplifying the above equation gives us the signal, whose instantaneous frequency f_i is given by

$$f_i = \frac{2v}{C} f_c + B f_r t_0 \quad (4.6)$$

where $t_0 = 2R_0/C$ has embedded in it, information about range in the first chirp used for measurement. Also, the term $2v f_c / C$ contains the information about the velocity of a target. However, since C has a high magnitude, the velocity term is much lesser than the range term. Therefore, measuring velocity from a single chirp is not possible. In order to do so, we need to transmit a series of chirps. We examine the approach to evaluate range and velocity in the next section.

4.2 Measuring Range and Velocity

In this section, we will attempt to understand intuitively, the approach to evaluate the range and velocity of a target. This will enable us to localise targets on a 2-D map, indexed by range and velocity. Such a 2-D map is referred to as a *range-doppler profile* or *range-doppler heat map*. Before we proceed to evaluate the range and velocity, we digitise the IF signal to facilitate further processing.

4.2.1 Evaluating Range

At the end of the previous section, we had understood the form of the signal appearing at the output of the low pass filter, and what information is embedded in this signal. Let us examine this again, but diagrammatically. Figure 4.4 shows the transmitted, received and mixed signals. As seen before, the output of the mixer signal contains a single tone or frequency. The value of this frequency can be evaluated by taking a simple Fourier Transform of the received signal at the output of the mixer. The natural question to ask next is what happens

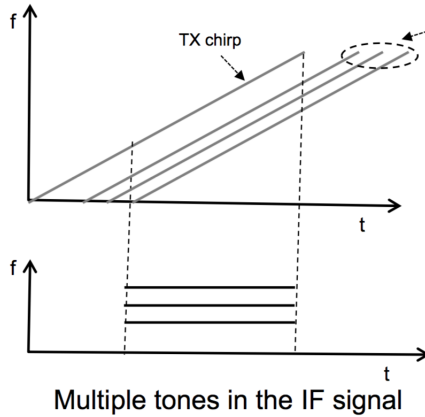


Figure 4.5: Transmitted, received and mixed signal outputs for multiple targets

if there are multiple targets? If we examine equation 4.6 one can see that this frequency is a function of range, and if there are targets at multiple ranges, there should be corresponding frequency components as well, and that is the case in practise. The presence of multiple targets at different ranges is indicated by different values of intermediate frequencies appearing in the mixed signal. This is shown in figure 4.5. Again, these frequency components can be evaluated by taking a Fourier transform over the output of the mixer signal.

The range of targets within a radars field of view, is measured by taking the Fourier Transform of the signal at the output of the mixer, for one transmitted chirp

The maximum range that can be measured is limited by system constraints such as the sampling frequency of the analog to digital converter at the receiver. If we use a complex baseband architecture as described in [19], the sampling frequency itself is the maximum intermediate frequency measurable. Thus, we can write a relation between the sampling frequency f_s , and maximum measurable range d_{max}

$$f_{if} = f_s = \frac{2Sd_{max}}{C} \quad (4.7)$$

where

$S = B/T_c$, is the slope of the chirp. The range resolution d_{res} now, can be viewed as the minimum separation between the intermediate frequency components for them to show up as discrete peaks in the Fourier domain. It is mathematically given by

$$d_{res} = \frac{C}{2B} \quad (4.8)$$

After taking the Fourier Transform over one chirp, the resulting frequency bins are referred to as range bins, as each frequency bin is indicative of a different range in space.

4.2.2 Evaluating Velocity

In equation 4.6 we had seen that there is a second term containing the velocity of the target. It was seen that due to its small magnitude, it cannot be separated by taking a Fourier Transform over a single chirp. We also saw that in order to detect this term, we need to process the signal over multiple chirps. We now discuss the methodology to extract this information.

We can simplify the intermediate frequency signal to correspond to the following form

$$v_m(t) = A \cos[2\pi f t + \phi_0] \quad (4.9)$$

where ϕ_0 is the phase term. Upon comparing this with equation 4.6, we see that $\phi_0 \equiv 2v f_c / C$. Thus, the velocity term or doppler term is responsible for causing a phase shift in the received signal.

In practical scenarios, the chirp time T_c is of the order of 10^{-6} s. In this interval, an object does not move by a significant amount. Thus, the intermediate frequency does not change much across chirps, but there is a significant change in phase due to the velocity. Let us understand this with a motivating example. Consider a chirp with $T_c = 40 \mu\text{s}$, slope $S = 50 \text{ MHz}/\mu\text{s}$, a centre frequency $f_c = 77 \text{ GHz}$. If the position of an object changes by 1 mm (corresponding to movement by $\lambda/4$), the change in IF frequency δf is

$$\Delta f = \frac{2S\Delta d}{C} = 333 \text{ Hz}$$

which corresponds to just $\Delta f T_c = 0.013$ cycles. However, the change in phase $\Delta\phi$ is given by

$$\Delta\phi = \frac{4\pi\Delta d}{\lambda} = \pi = 180^\circ$$

We observe that there is a significant change in phase but a negligible change in the IF frequency. This means, if we take a Fourier Transform to evaluate range over each chirp, the behaviour of the range bins across chirps will stay nearly the same. The only difference, would be the phase corresponding to these range bins across chirps. This phase is related to the doppler frequency. Thus, in order to evaluate the velocity of a target at a given range, we need to take the Fourier Transform of the corresponding range bin, across chirps. Since we deal with digitised signals, the Fourier Transforms are performed by using the Fast Fourier Transform algorithm or FFT.

As was the case with range, we have expressions for the maximum detectable velocity and the velocity resolution. Maximum detectable velocity is given by

$$v_{max} = \frac{\lambda}{4T_c} \quad (4.10)$$

and the velocity resolution v_{res} is given by

$$v_{res} = \frac{\lambda}{2NT_c} \quad (4.11)$$

where N refers to the number of chirps transmitted. The set of chirps, are also referred to as a frame. That is, the frame time $T_f = NT_c$, for a signal with 100% duty cycle. From the above equations we see that more the number of chirps, finer the velocity resolution. Also, smaller the chirp time, larger the v_{max} . In the next subsection we formalise the discussion further by arriving at an algorithm to evaluate the range doppler profile.

4.2.3 Algorithm To Evaluate Range-Doppler Profile

In the previous two subsections, we understood the basic intuition behind the technique used to evaluate the range and velocity. Now, we put these methods together in a single algorithm to evaluate the range doppler profile.

The mixer, produces an IF signal corresponding to each set of transmit and receive pulses which is digitised by the ADC. Let us store the digitised signal for each such set into the rows of a matrix. Thus, we now have a $m \times n$ matrix, given by

$$A = \begin{bmatrix} a_{11} & \dots & a_{1n} \\ \vdots & \ddots & \\ a_{m1} & & a_{mn} \end{bmatrix} \quad (4.12)$$

Where, m is the number of chirps transmitted, and n is the number of ADC samples

We first take a Fourier Transform across each row of this matrix. To make computation and representation simpler, we assume that the number of ADC samples is a power of 2. This first FFT gives us the location of targets in range, and will stay nearly constant across all chirps as typical chirp times a small. Now, among the n frequency bins (range bins), we find those having targets of interest and apply a second FFT along the column. This resolves the doppler components, and results in peaks having significant velocity components. The frequency bins along the columns, are now known as the velocity or doppler bins. At the end of this step, we now have the range-doppler profile. Figure 4.6 pictorially depicts this process. We represent our approach by writing pseudocode in Algorithm 1.

In the next section, we will briefly touch upon the measurement of the angle of arrival. We follow that with a discussion on chirp design, and some tradeoffs that we need to keep in mind during the design process.

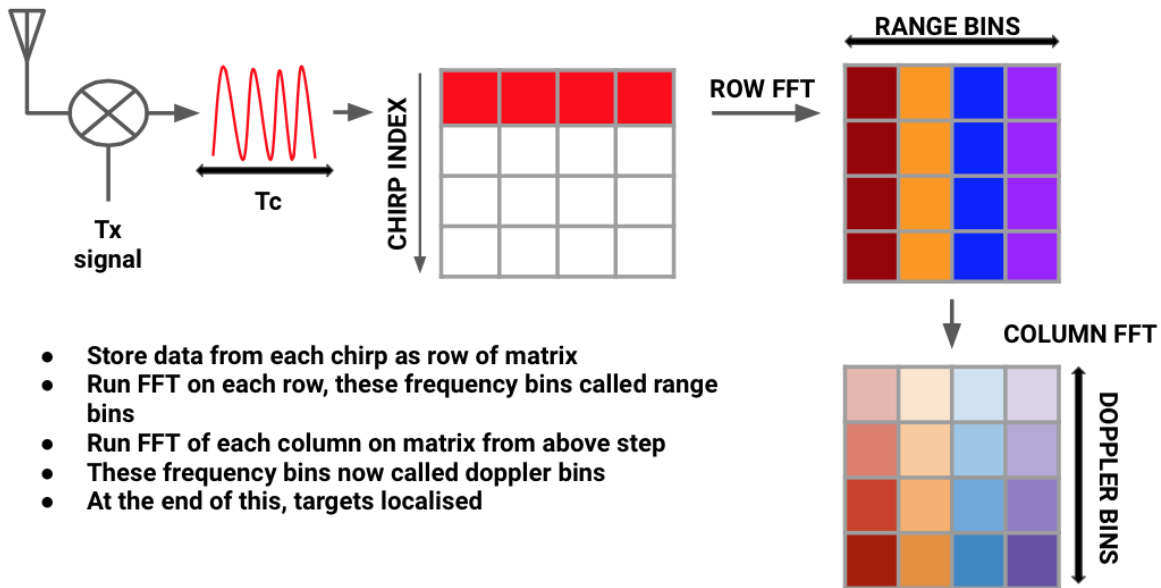


Figure 4.6: An illustration of the steps required to obtain the range-doppler profile

Algorithm 1 Range - Doppler Profile

Input: The received signal data for each processing frame

Output: The range-doppler profile of the targets in the field of view of the radar

```

1: procedure RDoppler(rxsig)                                ▷ Resolves range and velocity of targets
2:   for each row ri in rxsig do
3:     ri  $\leftarrow$  FFT(ri)
4:   end for
5:   for each column cj in rxsig do
6:     cj  $\leftarrow$  FFT(cj)
7:   end for
8:   rxsig  $\leftarrow$  ABS(rxsig)                                     ▷ take only magnitude of fft result
9:   rxsigdb  $\leftarrow$  MAG2DB(rxsig)                           ▷ range doppler profile matrix
10:  IMAGE(rxsigdb)                                         ▷ plot to visualise
11: end procedure

```

4.3 Measurement of Angle of Arrival

Thus far, we have managed to localise a target in terms of its range and velocity. What we also wish to know, is the direction along which the target is located. Evaluating the angle of arrival (AoA) helps us localise a target in terms of its angular position. In order for us to do so, we need at least two receiver antennas. The phase shift undergone by the signal between

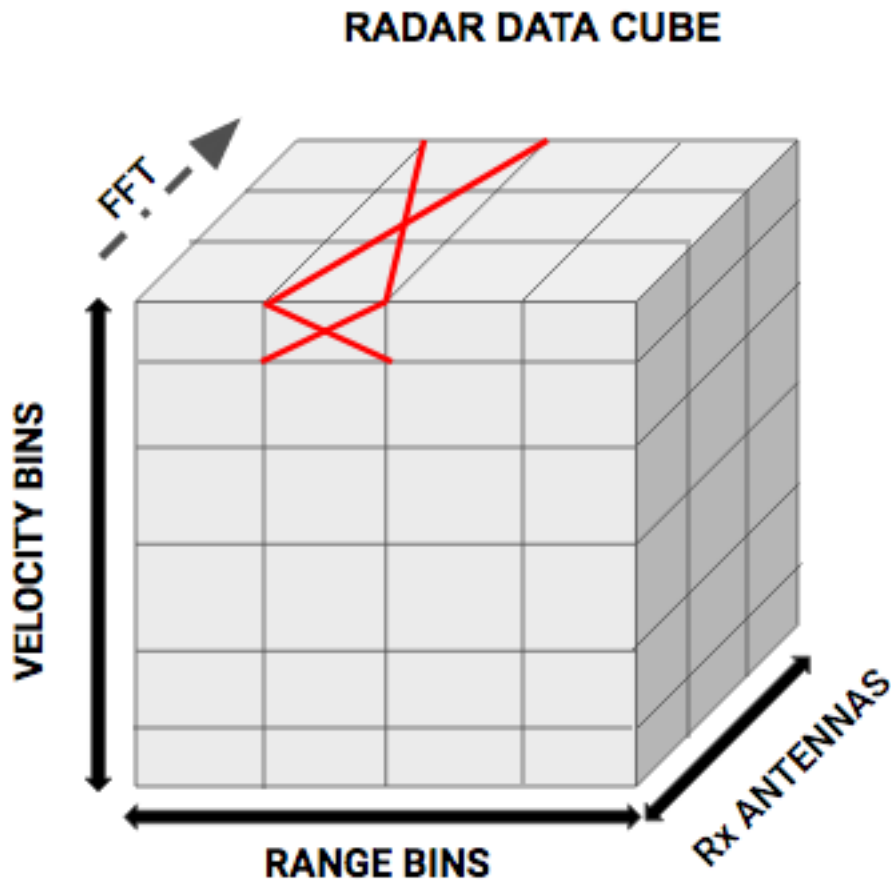


Figure 4.7: 3-D radar data cube with FFT of AoA evaluation shown

the two antennas, arising from the path difference between them is exploited to extract the information on AoA. A mathematical explanation of the same is available in [12]. A simple way to evaluate this angle is to use an FFT. This time however, we stack the range-doppler profiles into a cube, and apply the FFT over the third dimension of this cube as shown in figure 4.7.

4.4 Chirp Design

Thus far, we have understood the key parameters used in the operation of an FMCW radar. In this section, we try to map these parameters to those of a chirp.

Let us assume we are given the required range and velocity resolutions d_{res} and v_{res} , along with the maximum detectable range and velocity d_{max} and v_{max} . Let us also assume we are aware of the centre or start frequency f_c . The following procedure could be one used to design the chirp parameters

1. chirp time T_c can be determined from v_{max} from equation 4.10.

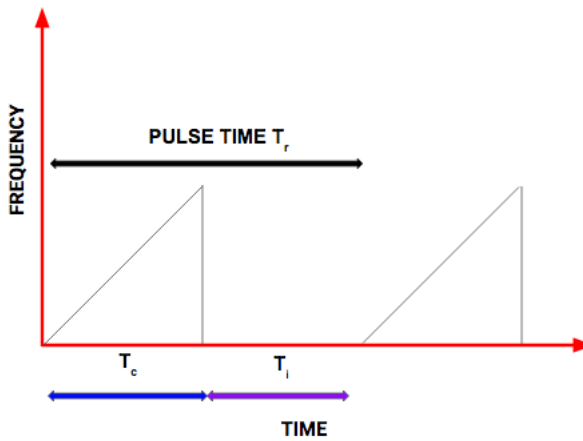


Figure 4.8: Frequency - time plot showing chirp time T_c , idle time T_i and pulse time T_r

2. Bandwidth B can be determined using the range resolution d_{res} using equation 4.8, thus slope of the chirp can be identified by using $S = B/T_c$.
3. Now, the frame time T_f can be deduced using velocity resolution v_{res} from equation 4.11.

This approach seems to work well in theory, but we might run into a few issues due to system constraints during implementation. For example, the sampling frequency f_s given by equation 4.7 might not be supported by the device. In this case, we might need a trade-off between d_{max} and slope S . Thus far, we have spoken of signals with a duty cycle of 100%. However, it may not be possible to generate such signals in practise. One reason for this could be that the system takes time to reset to the start frequency f_c after a sweep is completed. Also, the operation of the various subsystems such as the ADC and mixer must be synchronised. As a result of these constraints, there exists an idle time between two chirps, and the pulse time $T_r = T_c + T_i$ where T_i is the idle time between two chirps. This is represented diagrammatically in figure 4.8. One other constraint that must be considered is the amount of memory available to store data. To implement the algorithm discussed in the previous section, we need to buffer some data in memory. So, the maximum number of chirps that can be transmitted is dependant on the available memory.

The last tradeoff we will look at, is between d_{max} and d_{res} . Assuming we operate at the maximum sampling frequency f_s as given in equation 4.7, we can increase maximum detectable range d_{max} by reducing slope S . If we keep T_c constant, the reduced slope implies smaller bandwidth B , resulting in a poor range resolution, which can be seen from equation 4.8.

To conclude, in this chapter we looked at the basic operation and signal processing scheme for FMCW radars. In the next chapter, we understand the concepts discussed thus far through some simulations.

Chapter 5

Simulation Models

In the previous chapters, we understood the basics of radars and reviewed the operation of FMCW radars. In this chapter, we discuss two main simulation models: A simple target model, which approximates targets to a single point, and a point cloud model to help us model larger targets with significant area. The aim of these simulations is to understand the working of the algorithms we have described in the previous chapter.

5.1 Simple Target Model

In this section, we discuss the simple target model. We assume such targets to have a unity radar cross section. The objective of this model is to study the concept of range and velocity resolutions, and the range-doppler profile, as arrived at using algorithm 1 in chapter 4. For this model, we consider two targets with the range resolution d_{res} , maximum range d_{max} and maximum detectable velocity v_{max} being fed in as inputs. The required sweep bandwidth to realise the given resolution, is computed as per equation 4.8 in chapter 4. We assume for now that our system does not employ a complex baseband architecture, then we can replace f_s in equation 4.7 of the previous chapter with f_{if} , the maximum IF frequency which can be detected. In order to define the dynamics of the target, and the characteristics of the environment surrounding the target, we use the *PhasedArray* toolbox provided by MATLAB. As discussed at the beginning of this section, we keep the radar cross section to be unity. We now examine some of the results obtained from such simulations.

5.1.1 Single Target

We run the simulation to obtain the range-doppler profile for a single target. We take the centre frequency to be 77GHz, maximum detectable range resolution $d_{res} = 1\text{m}$, $v_{max} = 70\text{km/hr}$, and velocity resolution $v_{res} = 3\text{m/s}$. We let our target be located at a range of 10m, moving with a velocity of 10m/s. The range doppler profile obtained is shown in figure 5.1. As a special case, we change the range of our target to a value outside the maximum

detectable range. The result of this experiment is shown in figure 5.2

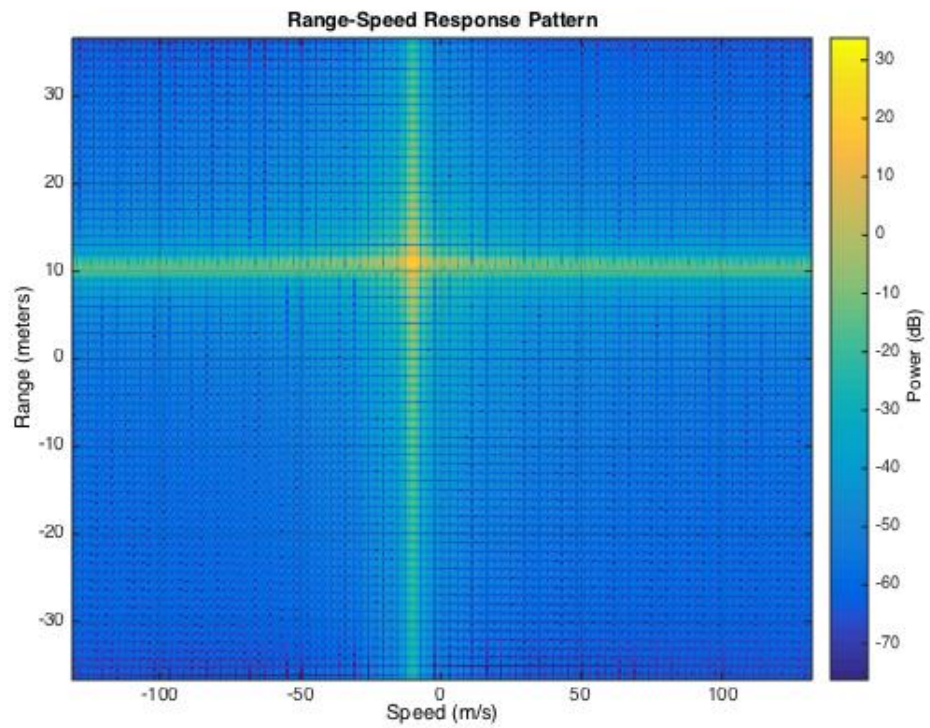


Figure 5.1: Range-doppler profile for a target located at 10m with a velocity of 10m/s

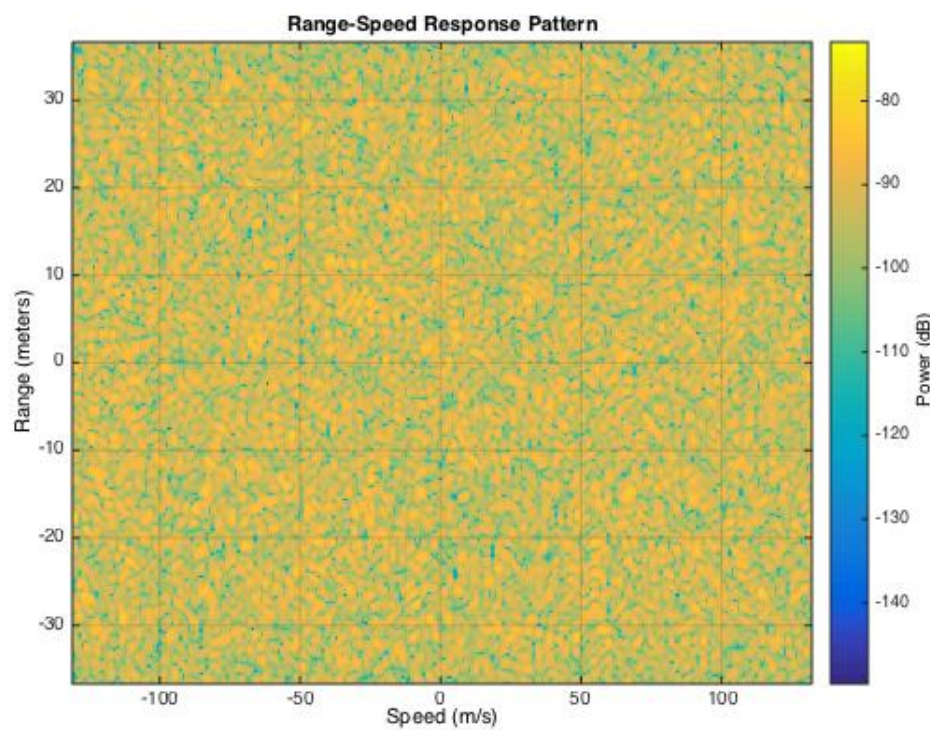


Figure 5.2: Range-Doppler profile of a target outside the maximum detectable range

5.1.2 Two targets

We now introduce a second target to this model. The system parameters stay the same as those described in the previous section. We begin by keeping targets at 5m and 8m, moving with velocities of 10m/s and 20m/s. The result of this simulation is shown in figure 5.3.

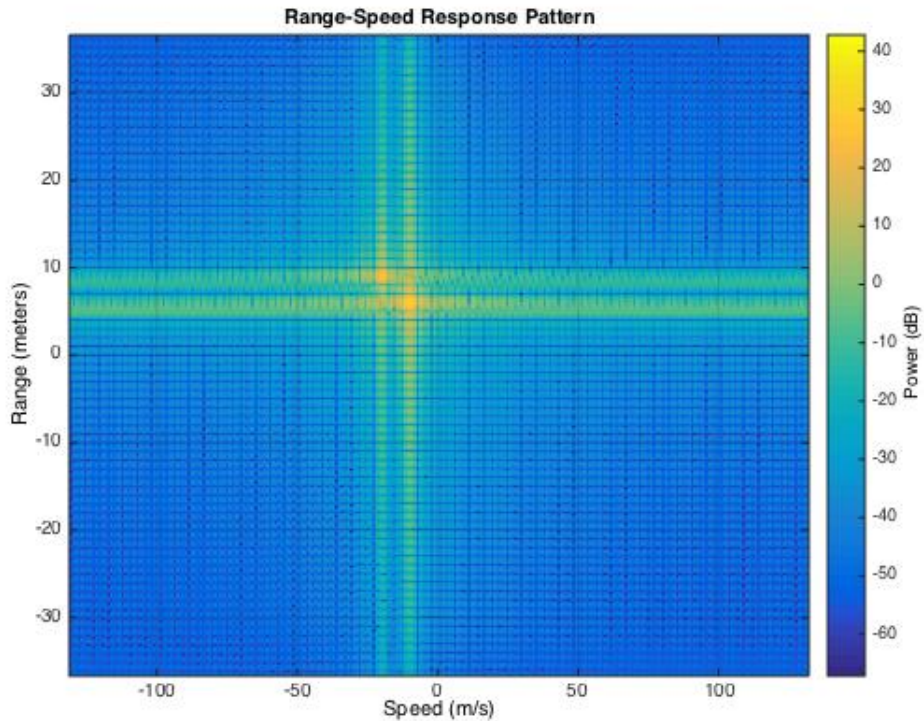


Figure 5.3: Range-doppler profile for two targets at 5m and 8m, moving with velocities 10m/s and 20m/s

We now see what happens if the separation between objects is smaller than the range resolution. To demonstrate this better, let us assume the targets are at the same velocity. We let the ranges be 5m and 5.5m, with a velocity of 10m/s. The result of this is shown in figure 5.4. As expected, the two objects are unresolvable. However, if they move with different velocities, say 10m/s and 20m/s they are resolved as separate targets, as shown in figure 5.5. We next consider two objects at different ranges, moving with the same velocity. Let the targets be located at 15m and 20m, with a velocity of 20m/s. Simulating with these parameters gives the range doppler profile as in figure 5.6. The last configuration we try simulating is two targets located at the same range, with different velocities having a difference lesser than the velocity resolution $v_{res} = 3\text{m/s}$. The results of this simulations are shown in figure 5.7

Through this model, we managed to study the the range-doppler profile. The drawback however is that we cannot model targets with uneven shape. In achieve this, and study the decay in received power with distance, we introduce a new model in the next section.

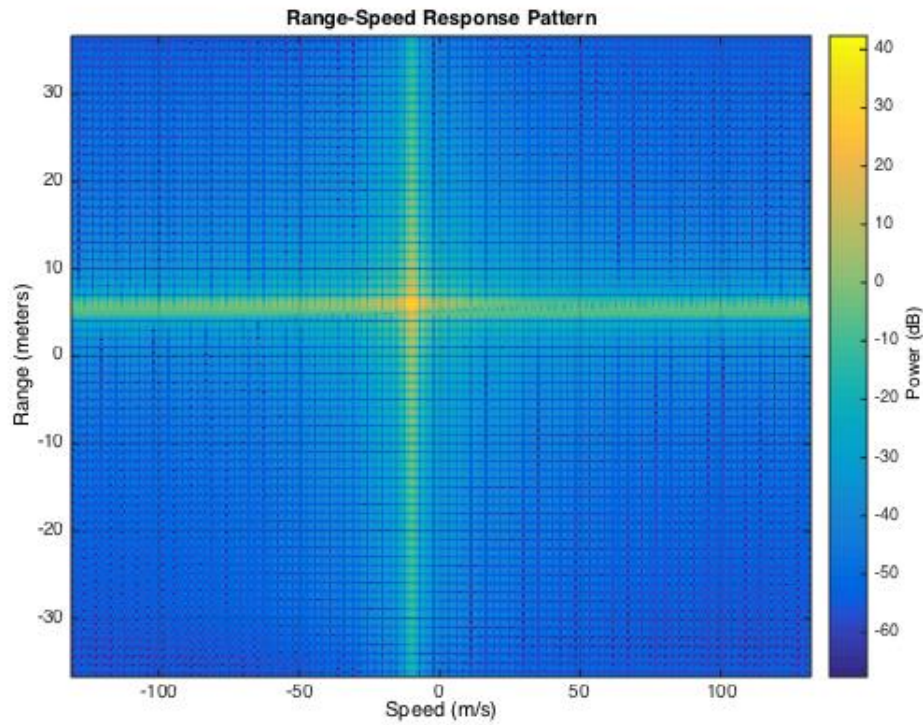


Figure 5.4: Range-doppler profile for two targets at 5m and 5.5m, moving with a velocity of 10m/s

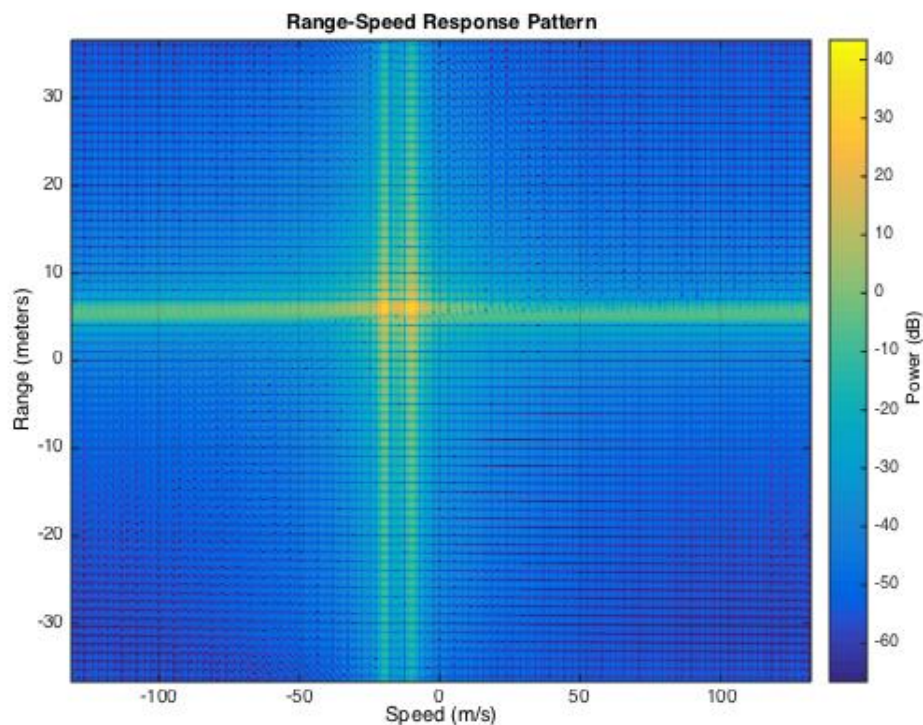


Figure 5.5: Range-doppler profile for two targets at 5m and 5.5m, moving with velocities 10m/s and 20m/s

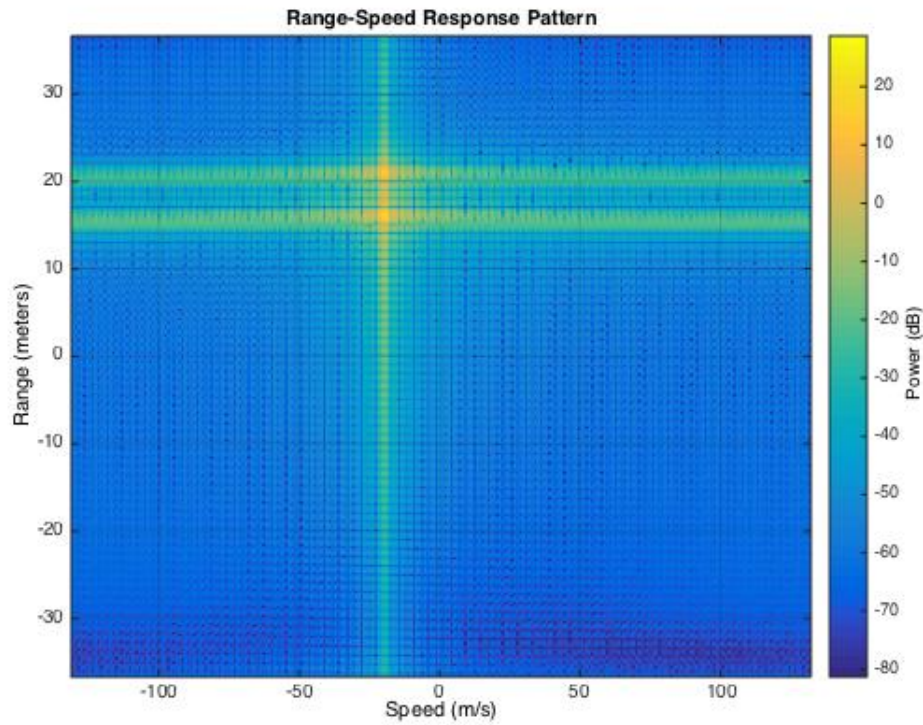


Figure 5.6: Range-doppler profile for two targets at 15m and 20m, moving with velocity 20m/s

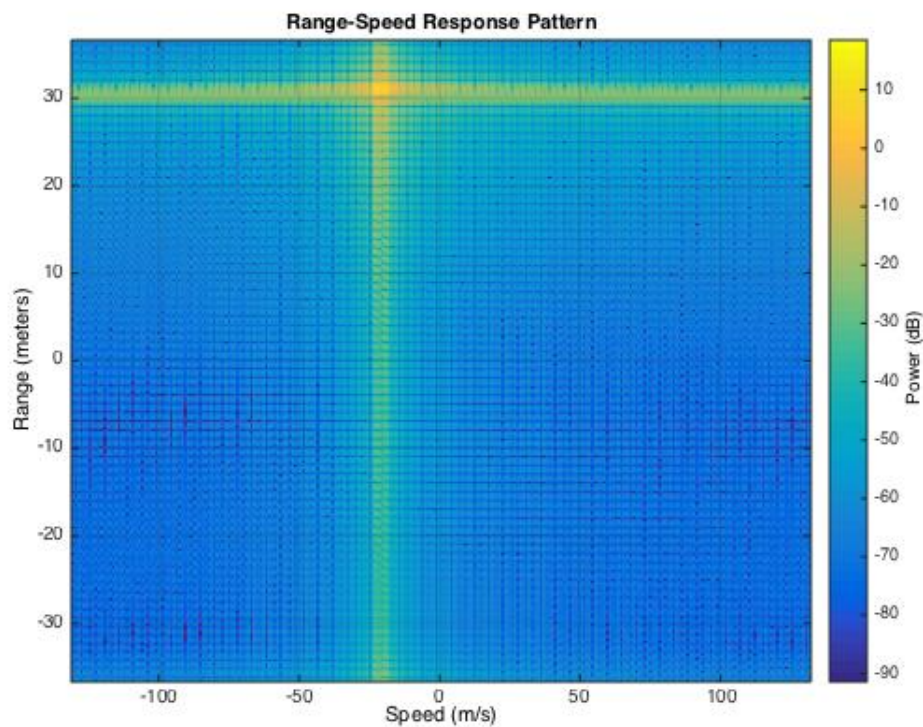


Figure 5.7: Range-doppler profile for two targets at 30m, moving with velocity 20m/s and 22m/s

5.2 Point Cloud Model

The main objective of the model includes

1. Study targets with different surface areas and shapes.
2. Study the decay of power with range, i.e., the inverse square law as described in section 2.3 of chapter 2.

A diagrammatic description of this model is given in figure 5.8. Here, the space within the field of view of the antenna is divided into a grid, with each cell addressed by its range, and azimuth angle. Targets are modelled as a collection or *cloud* of points. These points are placed within each desired cell in the grid. The key parameters that need to be modelled include

1. Range loss, which from equation 2.2 of the second chapter is inversely proportional to the square of the distance. i.e., $R_{loss} \propto \frac{1}{4\pi R^2}$.
2. Reflection coefficient of target: 100% of the incident signal is reflected off a target. Negligible fraction of incident power is scattered off the rest of the cells in the grid. This helps us model background clutter.
3. Time delay: As discussed in the earlier sections, the time delay is modelled as $\tau = \frac{2R_{target}}{C}$.

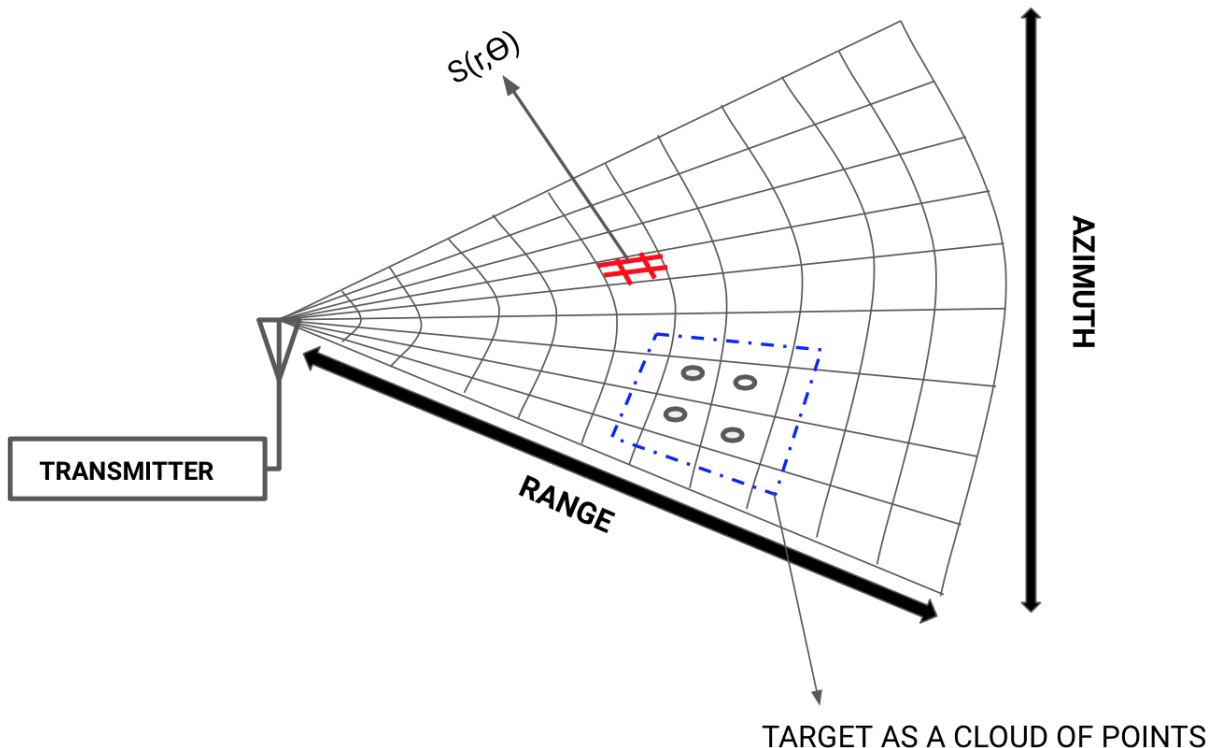


Figure 5.8: Proposed point cloud model

The model is implemented by constructing a matrix of dimension $a \times b$ where a is the number of range points considered, while b the number of azimuth points considered. We first define the position of each target within this matrix, and the individual cells they occupy. This is followed by defining the above three parameters for each cell in the grid. Now, this model is integrated with the signal processing framework for FMCW radars established in chapter 4 and range analysis is performed. The key limitation of this model is the inability to efficiently model velocity. The reason being, introducing velocity requires to update the position of the target points in the matrix which is not a trivial operation. Also, the grid sizes need to be varied as per the desired velocity resolution. Thus, the purpose of this model is restricted to understanding the behaviour of static targets. We now look at some simulation results from this model.

5.2.1 Single Target

In this section we study the behaviour of a single target placed in front of radar under different conditions.

Let us assume that a single target is located at a distance (range) of 4m in front of the radar, along the 0° azimuth. The area of the target is $0.02m^2$. As described before, we construct the range-azimuth matrix and integrate with the signal processing scheme described by algorithm 1 from the previous chapter. Figure 5.9 shows the results of this simulation. Here, we have plotted the range profile, and the reflection coefficient as a function of the target range and azimuth. We observe that the value of reflection coefficient is significantly higher where the target is present, as compared to the surroundings. The fall in the level of received power with increasing distance can also be inferred from this graph. Now, If this target changes azimuth to -10° , maintaining the same range, the results obtained are as given in figure 5.10. It is observed that there is a change in location of the target along the azimuth, i.e, the angular position relative to the radar has changed, but the radial distance from the radar, or range remains to be the same.

If we examine the range profile, we notice there are smaller peaks that appear at locations other than where the target is located. These have negligible magnitude when compared to the main peak, but are still non-zero. This is a consequence of associating a minuscule value of reflection coefficient with each cell in the matrix. This is how we model stray scatterers or clutter in the system.

In the next section, we examine what happens when we introduce multiple targets. There, we will study the effect of varying target areas, having targets located at different positions along the azimuth and show that if an object is located at a far distance from the radar, it may be a possibility that this target may get masked by the clutter.

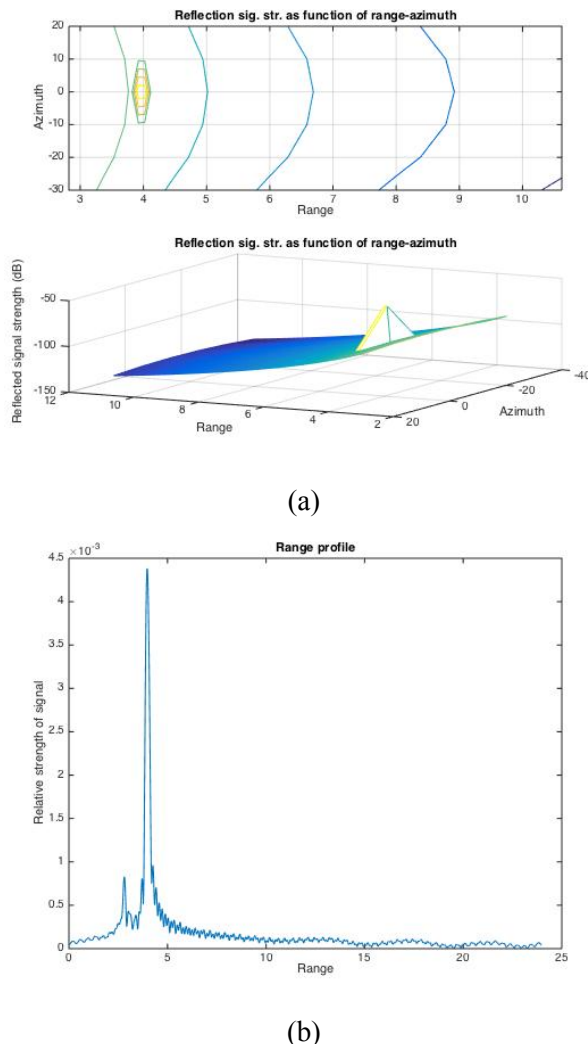


Figure 5.9: (a) The reflection coefficient is plotted as function range and azimuth (b)The range profile indicates the presence of a target at the given range

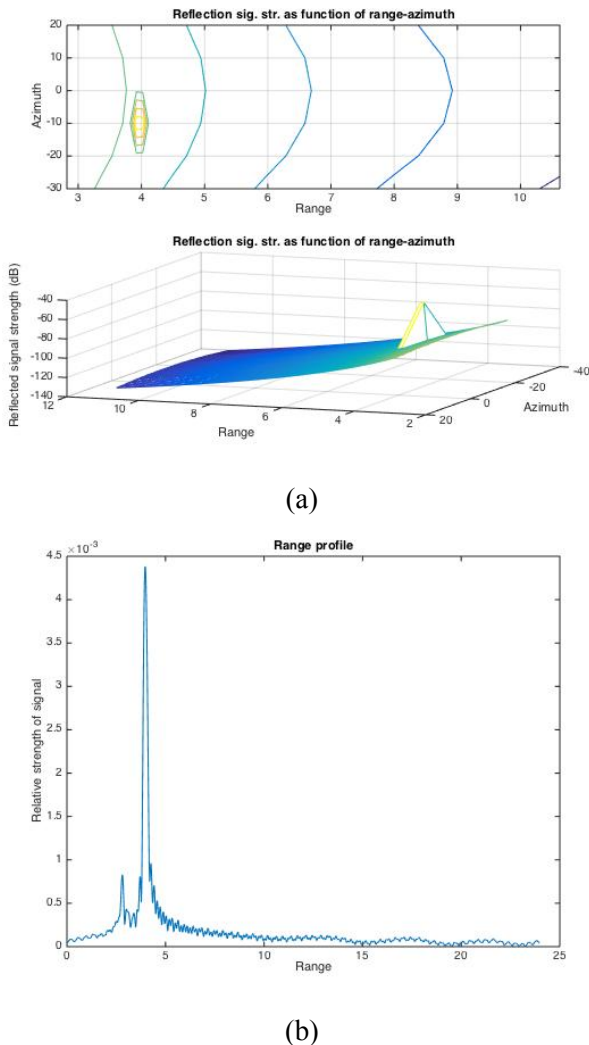


Figure 5.10: (a) The reflection coefficient is plotted as function range and azimuth. Notice there has been a change in target azimuth (b)The range profile remains the same, indicating the change in azimuth has not impacted the range

5.2.2 Multiple Targets

In this section we examine the effect of having multiple targets. We begin by placing three targets at 3m, 5m and 7m, at a 0° azimuth. The area of each of these targets is kept to be 0.02m^2 . We apply this to our model, the output of which is shown in figure 5.11. As we did in the previous subsection, we now place our targets at different azimuth angles of -10° , 0° , 10° respectively, while maintaining their range. Figure 5.12 shows the the range profile and contour map of such a configuration. The last experiment we try, is to see the effect of increasing target areas. We maintain the same configuration as in the previous case. The result of this simulation is shown in figure 5.13

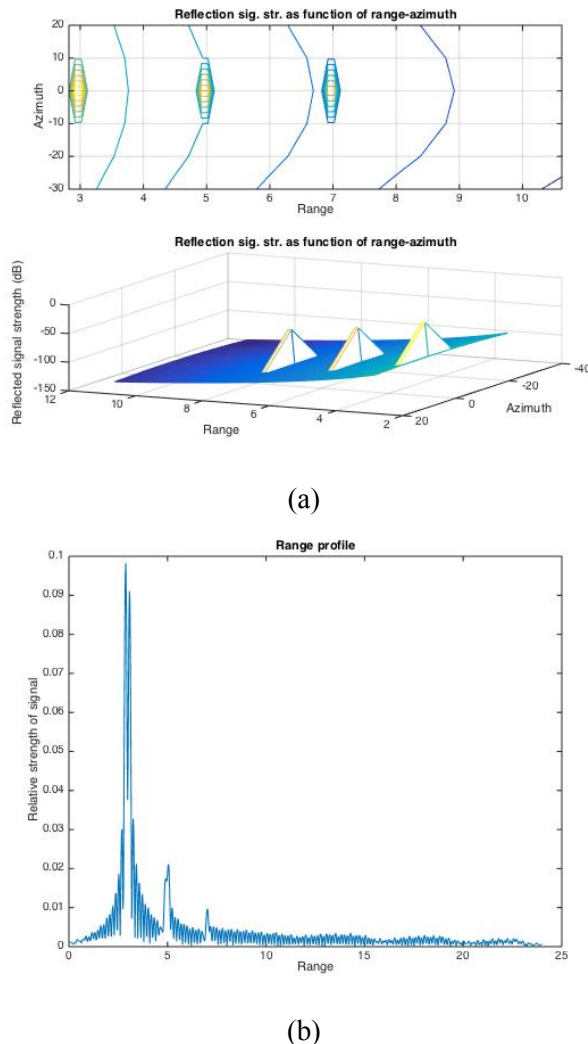


Figure 5.11: (a) The reflection coefficient is plotted as function range and azimuth. (b) The range profile shows the three targets, with the signal strengths reducing with moving distance

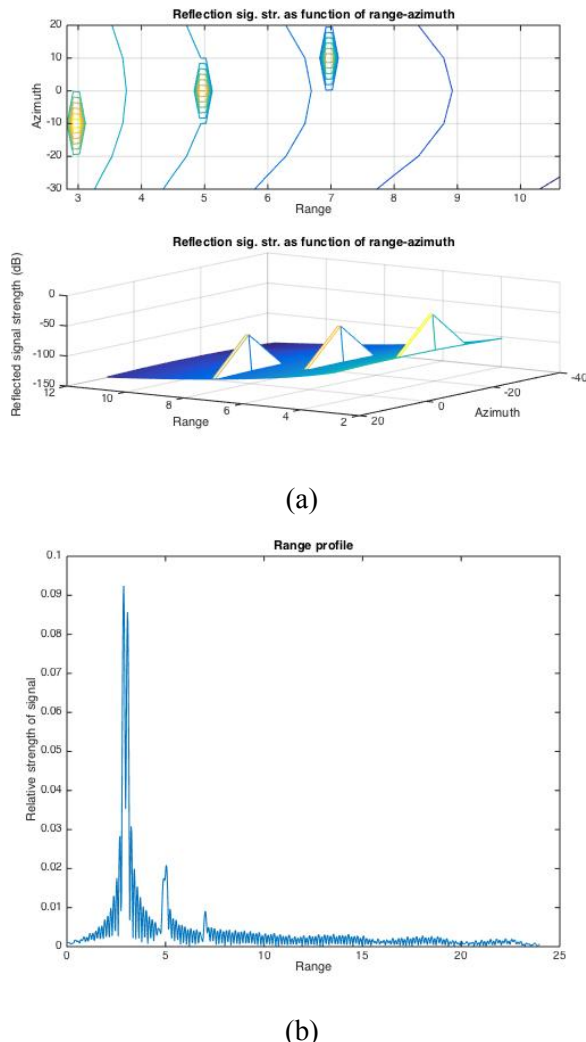


Figure 5.12: (a) The reflection coefficient is plotted as function range and azimuth, notice the change in azimuth position in the contour map (b)The range profile shows the three targets, with no change from before

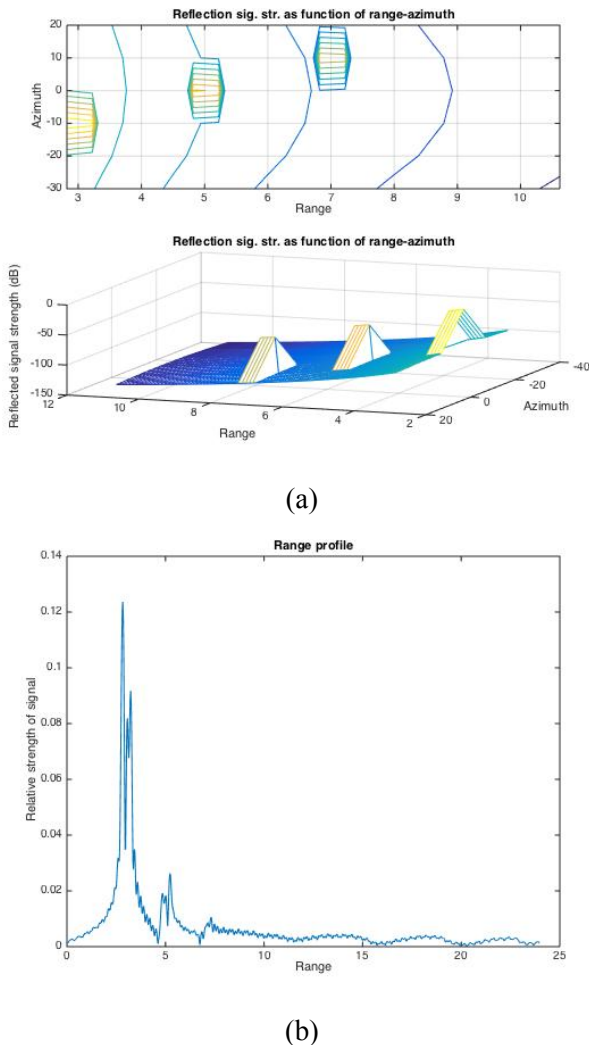


Figure 5.13: (a) The reflection coefficient is plotted as function range and azimuth, notice the the spread of the target due to their larger areas (b)The range profile does not show the targets so distinctly, as they occupy more range bins, and may be blocked by the presence of the first target

Thus far, we have discussed the theory of FMCW radars, and understood its working through simulations. We have been able to identify the range and velocity of targets. The IF signal at the output of a mixer contains frequency components corresponding to the range, while the doppler shift introduced in this signal carries information about the velocity. Until now, we have discussed the translational motion of a target. It may occur that a target has a rotational motion, or other moving components which do not impact the range. To achieve our end objective of distinguishing between rotating and non-rotating targets, identifying such motion is important. In the next chapter, we discuss the mathematical tools required to study such motion, called as *micro-motion*.

Chapter 6

Analysis of Micro-Motion

A target with a net translational motion may possess smaller moving components. The rotating blades of a helicopter are the best example. These rotate about a fixed point, while the helicopter as a single object moves forward. A bird flapping its wings in flight is another example of a moving body with smaller moving parts. The motion of these small components is called micro-motion. In this chapter, we study micro-motion and its effect on the doppler frequencies.

6.1 Micro-Motion and The Doppler Effect

From equation A.5 in appendix A, the relation between the velocity of an object and the doppler frequency is given by

$$f_d = \frac{2v\cos(\theta)}{\lambda}$$

Here, the velocity $v\cos(\theta)$ is the radial velocity, along the line of sight joining the radar and target. Now, if all components of the target move with the same velocity v , the doppler frequency f_d stays constant. However, if this velocity changes due to micro-motion, the doppler frequency also changes. Since we are interested in studying rotating targets, we take the example of the rotor blades of a helicopter to understand this better. Consider a simplified setup shown in figure 6.1. Here, v_t is the tangential velocity of the rotor blade at a given point. This velocity is resolved into its orthogonal components along the X and Y axes as shown. When the rotor blade rotates by a small amount, the direction of the velocity changes(i.e, θ changes), as a result of which the magnitude of velocity along the radial direction, $v\cos(\theta)$ changes. As a consequence of this, the doppler frequency f_d changes. Since rotation is a form of periodic motion, the variation in doppler frequency is also periodic in nature. One can see, that other forms of motion such as a bird flapping its wings, or vibrating components of a machine must also produce similar variations in doppler frequency. This variation in doppler frequency caused due to micro-motion is termed as the micro-doppler effect [21]. In the event of this moving component being part of a larger ob-

ject with translational velocity, this variation in doppler will be about the principal doppler frequency due to this velocity.

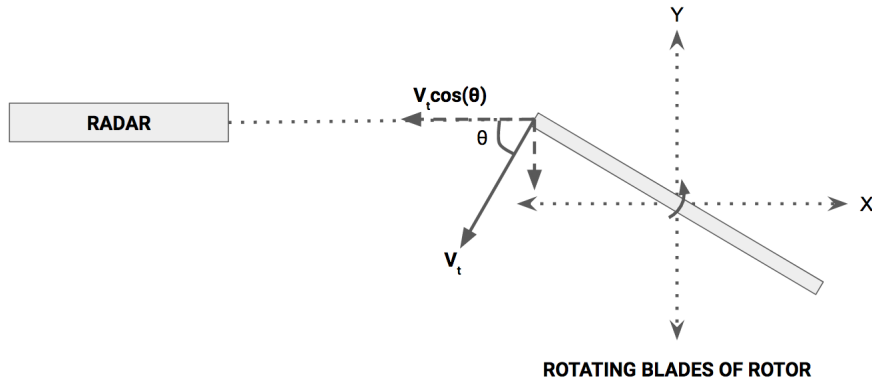


Figure 6.1: Simple diagram of rotor blade to illustrate change in doppler frequency

In the next section, we discuss signal processing techniques to study the micro-doppler phenomenon along with relevant results from literature.

6.2 Micro-Doppler Analysis

In this section we discuss the signal processing tools required to study the micro-doppler effect. Intuitively, one might think that the Fourier Transform taken to resolve a target's velocity must suffice for this case. Let us understand the information given to us by the Fourier Transform to understand why that is not true. The Fourier Transform tells us what frequencies appear in a given signal across a time interval T , without any information about the time instants at which these frequencies appear within this duration. This temporal localisation is important to us, because that can give us information about the dynamics of a target with micro-motion. We achieve this time localisation by using time-frequency (TF) distributions to analyze the signal. The reader can refer to the textbook on time-frequency analysis by Leon Cohen [14] for deeper insight into the topic. A brief introduction to various techniques discussed in this section is available in appendix B.

Rahman et al.[22] discuss an approach based on the Short Term Fourier Transform (STFT) to analyze the micro-doppler spectrum on simulated data. Here, the STFT is applied in place of the second Doppler Fourier Transform in algorithm 1 in chapter 4. They present the spectra for the moving blades of a helicopter and flapping of a birds wings as discussed before, and it is shown in figure 6.2. This figure shows the periodic variation in the doppler spectrum indicative of the periodicity in rotational motion, or the flapping of wings. In reality, a target would be moving with a velocity of its own, or even accelerating in time, as shown in figure 6.3. If we want to study the nature of the micro-motion, i.e., whether it

is rotational etc, we need to keep our observations invariant to the net translational or bulk motion of the target.

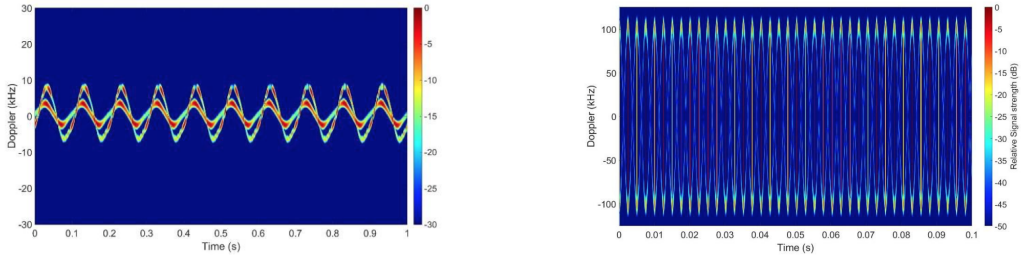


Figure 6.2: Short-Term Fourier Transform spectrum of (a) flapping wings of a bird (b) rotating blades of a helicopter. Source: S. Rahman and D. Robertson, “Time-frequency analysis of millimeter-wave radar micro-doppler data from small uavs”

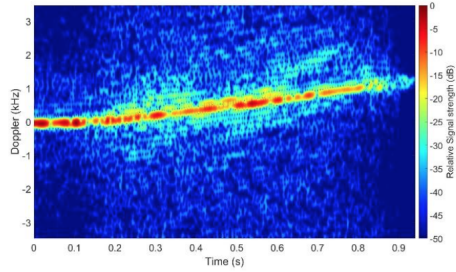


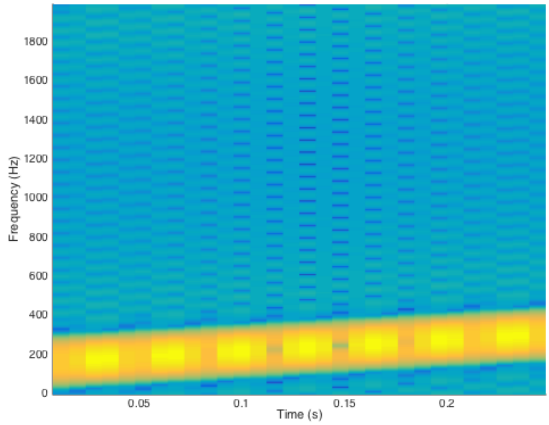
Figure 6.3: STFT of an accelerating target. Notice the variation of doppler frequency. Source: S. Rahman and D. Robertson, “Time-frequency analysis of millimeter-wave radar micro-doppler data from small uavs”

Molchanov [23] proposes a pipeline to extract micro-doppler information in cases where the target has a bulk translational motion. He suggests the following steps to be followed to extract the variation in doppler due to movement of small components on this target, after the range FFT has been completed in Algorithm 1.

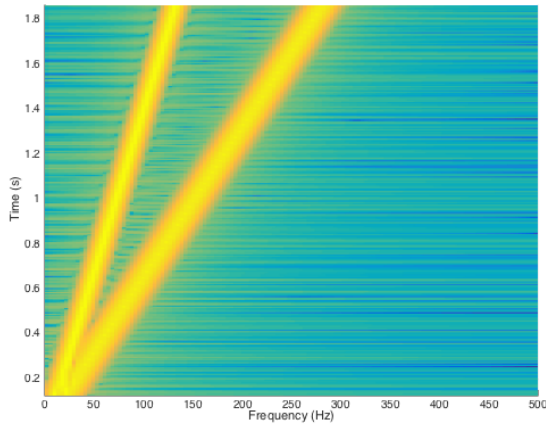
1. Transformation: Transform the range-bin data to be analyzed into time-frequency domain, to study how energy is distributed across various frequencies.
2. Filtering: Some time independent noise is introduced into the system due to the system and environment, can this needs to be filtered out. A technique such as spectral subtraction can be used for this purpose.
3. Alignment: Align the micro-doppler profile about the zero doppler, by removing the component due to the bulk motion of the target.

At the end of this stage, we have reduced all signals to vary about the zero doppler frequency, and can now be compared to analyze the nature of motion causing these signatures. The challenging step in the pipeline, is that of alignment. We must know the exact bulk velocity profile of a target. This is not easy to predict. The author designs an estimator to predict the

doppler frequency, and aligns the spectrum using this estimate. The disadvantage however, is that in the event of an error in prediction, the output could be highly erroneous. Apart from this, the procedure outlined above involves other challenges. If there are multiple targets moving with nearly same velocities and located close to each other, the signatures may appear to be the same. This could depend on the resolution of the TF distribution used for analysis [14], and is depicted in figure 6.4a. Another problem, could be that the signatures overlap in frequency at some point in time, as shown in figure 6.4b.



(a)



(b)

Figure 6.4: The two challenges associated with extracting micro-doppler signatures (a) inability to distinguish between two closely spaced signatures (b) signatures overlapping in frequency at some point in time

The first problem can arise due to poor time or frequency resolution of the TF distribution used to analyze the signals, and the tradeoff between the two resolutions. For example, a technique such as STFT has a poorer resolution compared to a technique like the Wigner-Ville Distribution. These aspects are discussed in appendix B. An approach to solve the second problem is discussed by Suresh et al. [13], where techniques such as Fractional Fourier Transform (FrFT) and Fourier Bessel Transforms (FBT) are used to isolate the sig-

nature of each target.

We discuss the concept of micro-doppler in detail, as it gives us the features required to classify targets using a radar. Thus far, we understood various theoretical concepts and techniques required to process the radar data. In the remaining chapters, we discuss the features of our sensor, visualise a few datasets collected using this sensor, and proceed to classify targets.

Chapter 7

Data Collection and Classification

Thus far, we have understood the fundamentals of FMCW radar signal processing and the concept of micro-doppler analysis. In this chapter, we will understand the features of the TI-AWR1642 millimeter wave radar sensor, which is used to collect data. This will be followed by an overview of datasets collected, features extracted from these datasets followed by a discussion on relevant classifiers.

7.1 The TI-AWR1642 Millimeter Wave Radar

The sensor that we work with is the AWR1642 EVM built by Texas Instruments. Shown in figure 7.1, the radar operates between the frequency band of 76GHz to 81GHz with a maximum sweep bandwidth of 4GHz. It has two transmit and four receive antennas, built as patch antennas on the board. Further details are available in the datasheet [7] and user guide [18]. In this section, we understand the procedure to be followed while extracting data from the sensor to the host computer and the challenges associated with it.

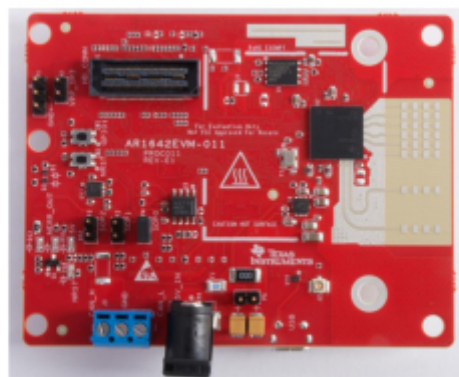


Figure 7.1: The TI-AWR1642 mmWave radar

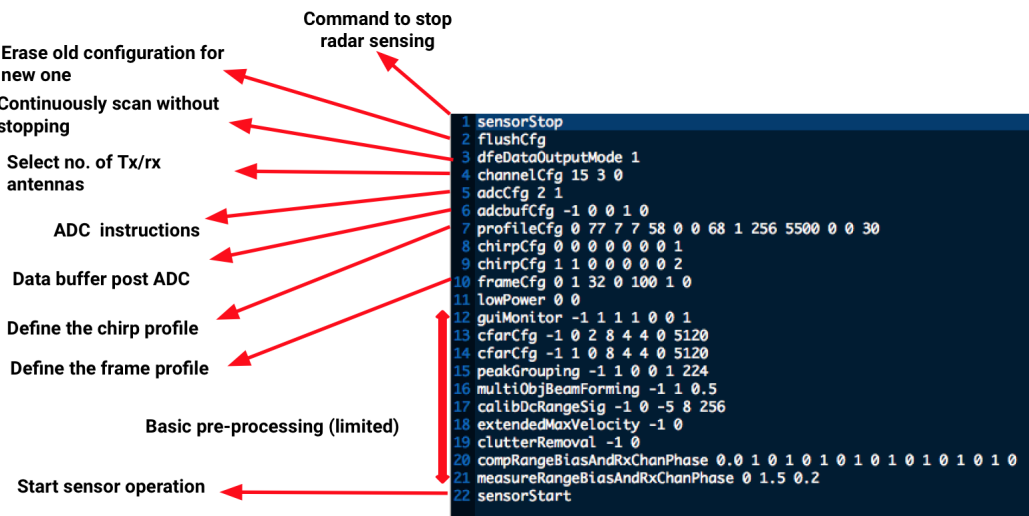


Figure 7.2: Sample configuration file with each field labelled

7.1.1 Controlling Sensor Operation

The operation of the sensor can be controlled using a configuration file. This is analogous to a program file, containing details about the desired chirp configuration, frame configuration, ADC information and so on. Figure 7.2 shows a sample configuration file with the meaning of each line. These fields are further explained in detail in the user guide [18].

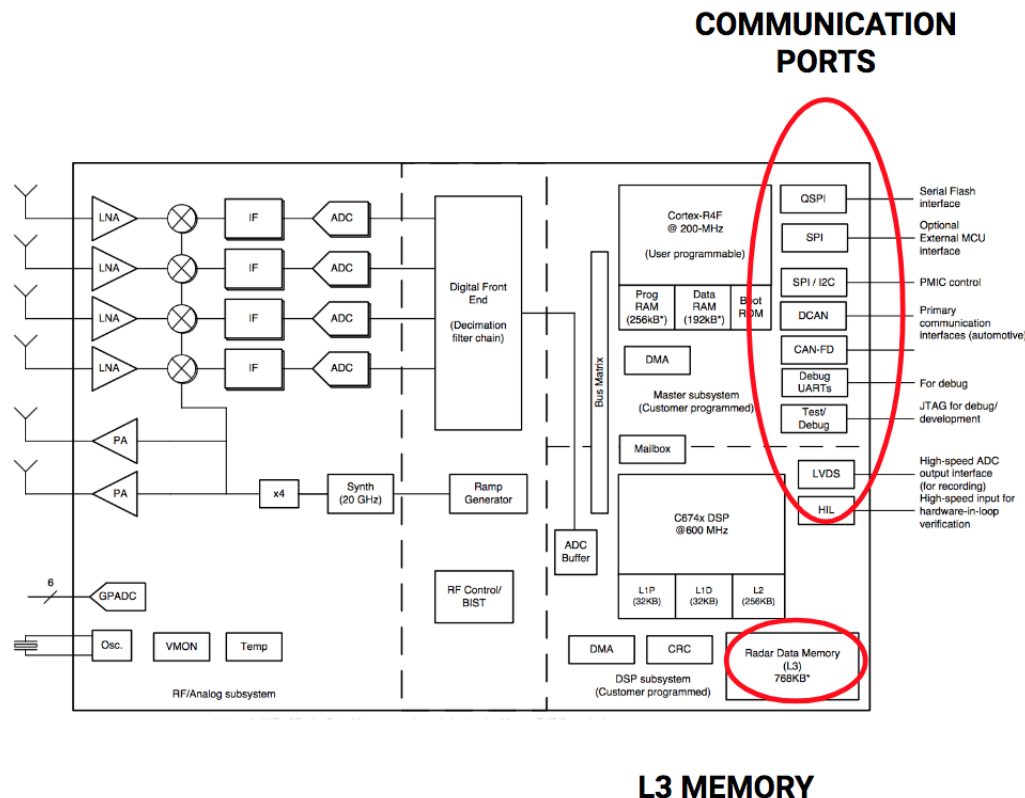
This configuration file is loaded onto the sensor. The command `sensorStop` terminates any ongoing operation, `flushCfg` erases the existing configuration to load a new one. The commands `chirpCfg`, `frameCfg`, `profileCfg` define the characteristics of the chirp such as the sweep slope, idle time and so on. The sensing operation commences when `sensorStart` is passed.

7.1.2 Data Extraction

The sensing operation commences upon passing the `sensorStart` command. The data collected by the sensor, is stored in a memory location called the L3 memory after some pre-processing. This includes the digitising of the IF signal and taking the Fourier Transform to obtain the range profile. The data is now able to be extracted from the board as a binary dump. To do so, the board provides support for communication protocols such as UART and SPI to transfer the data from the sensor to the host system. Figure 7.3 shows the location of the L3 memory and the various communication protocols.

There are a few challenges that need to be met in each of these steps: from sensing to data transfer, which we list below

1. Although the board supports configurations with different combinations of two transmit and four receive antennas, not all of them work. The reason for this behaviour is still being studied.



L3 MEMORY

Figure 7.3: A schematic of sensor with L3 memory and communication ports highlighted

- It is mentioned that protocols such as SPI are available to transfer data. However, there seems to be a gap in understanding the firmware for this protocol , and it runs into errors and crashes.
- Due to the inability to get SPI fully working, UART is the data protocol used to transfer information. This presents a challenge due to its low rate of data transfer. The L3 memory is overwritten every time a new frame of radar data is available. Thus, to prevent data corruption we must transfer this data before the arrival of a new frame. To satisfy this, only a maximum of 64kB of data can be transmitted. So, there is a tradeoff between the maximum detectable range and velocity due to this issue.
- Finally, the data extracted from the board is a binary dump. In order to parse through and correctly interpret the data, one needs an understanding of the memory architecture. In our case, since we deal with complex data, the real and imaginary parts are individually stored as 16 bit signed integers. So we read our data accordingly.

Efforts are being made to understand and solve these problems. In the next section, we take a look at some of the data collected using the sensor. Algorithms, and tools discussed in the previous chapters will be used to analyze and interpret this data.

7.2 Data Visualisation

In this section we examine the datasets collected using the AWR1642 sensor. These visualisations are obtained upon application of the concepts introduced in the previous chapters, namely the range-doppler profile and micro doppler analysis. After this stage, we proceed to extract some features from this data and then train a classifier to help us distinguish between rotating and non-rotating targets.

7.2.1 Dataset - I

This dataset is collected in an indoor environment as shown in figure 7.4. Table 7.1 lists the configuration parameters that are used in this exercise. We place metallic reflectors at 32cm and 168cm from the radar sensor, and observe the behaviour of the range profile.



Figure 7.4: A view of the environment for first round of data collection

PARAMETER	VALUE
Start Frequency	77GHz
Frequency Slope	100MHz/ μ s
Idle Time	739 μ s
Tx start time	0 μ s
ADC start time	7 μ s
ADC samples	64
Sample rate	2MHz
Chirp Time	40 μ s
Rx antenna gain	30dB
No. of chirps	32
Sensor orientation	0°

Table 7.1: Configuration parameters for round-1 of data collection

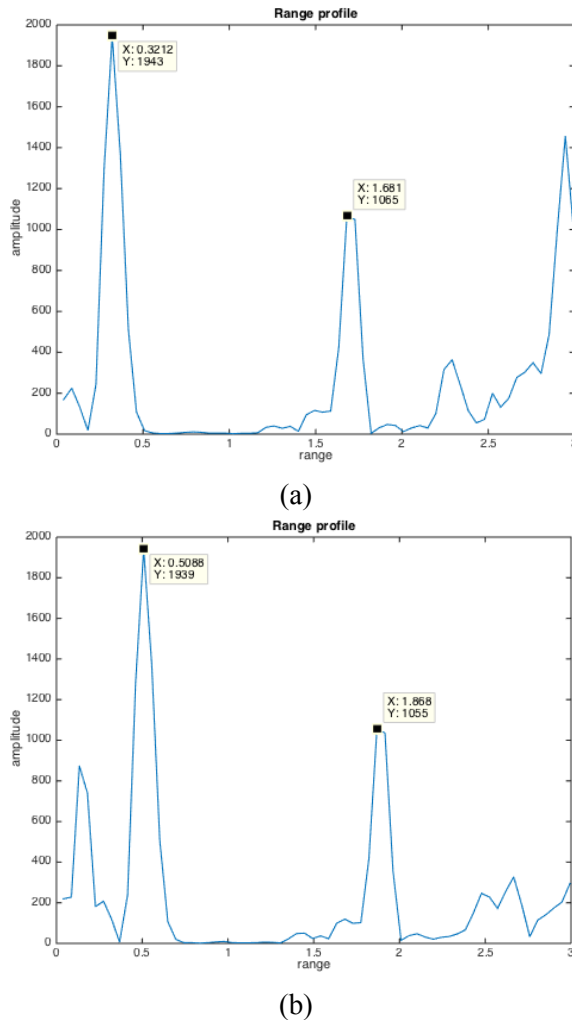


Figure 7.5: The range profile for two consecutive frames (a) and (b) is shown. There is a change in position of peaks even though no object is moving

Examination of figure 7.5 reveals there is an anomaly, as the position of the peaks changes between frames. Some investigation revealed that stray data was being appended to the beginning of each frame, due to improper flushing of the UART buffers. Therefore,

apart from the first frame, the data might be incorrect. For the next round of data collection, we rectify this mistake and move to an outdoor environment.

7.2.2 Dataset - II

For the second round of data collection, we move to an outdoor environment which is representative of the actual intended environment of application. A view of the environment is presented in figure 7.6. The configuration parameters that are used are mentioned in table 7.2. We take the range profile of the scene and study its characteristics.

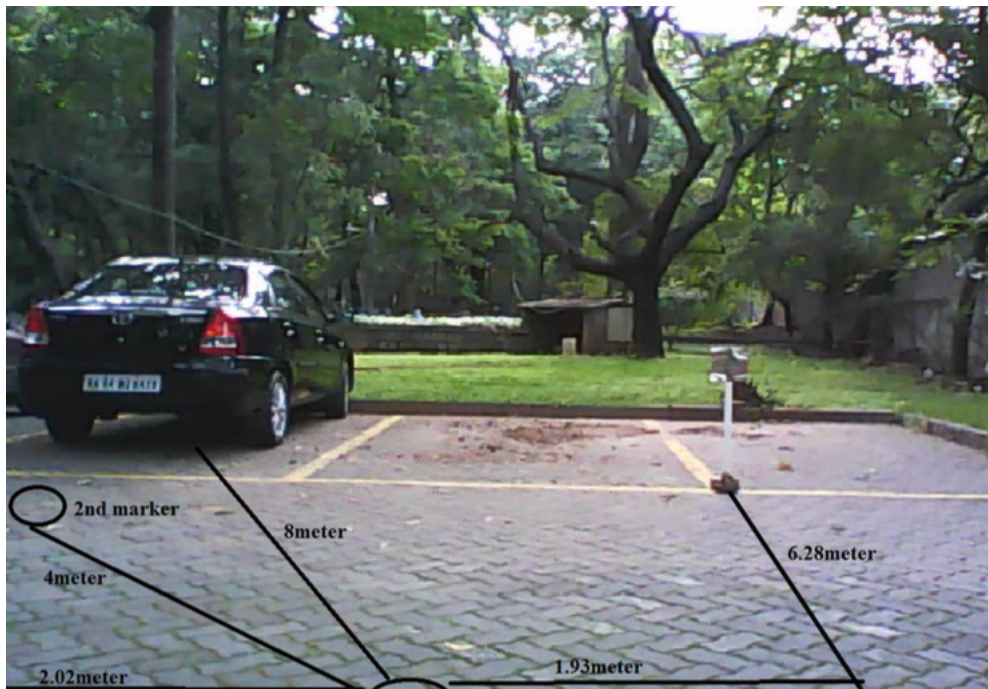
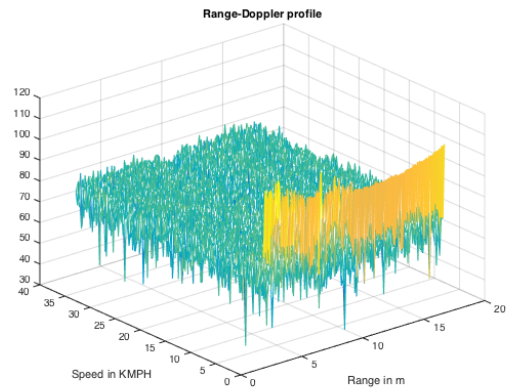


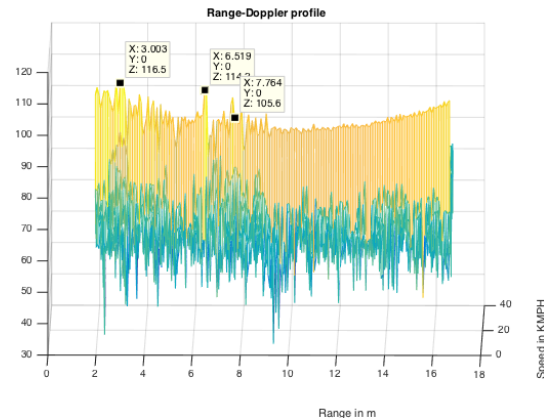
Figure 7.6: A view of the environment for the second round of data collection

PARAMETER	VALUE
Start Frequency	77GHz
Frequency Slope	64MHz/ μ s
Idle Time	10 μ s
Tx start time	0 μ s
ADC start time	6 μ s
ADC samples	256
Sample rate	8MHz
Chirp Time	45 μ s
Rx antenna gain	30dB
No. of chirps	128
Sensor orientation	10°down

Table 7.2: Configuration parameters for round-2 of data collection



(a)



(b)

Figure 7.7: (The range-profile for two consecutive frames (a) and (b) present two different views of the same. Notice there is a lot of clutter

Examining figure 7.7, we can observe one is unable to clearly distinguish between the target from the background. What is also peculiar, and contrary to expectation is there are high velocity components which appear, even though none of the targets are moving. This could be due to the multiple ground reflections and presence of clutter and other objects in

the background. There are a few possible steps which can be taken to address this problem.

1. The inclination of the antenna, or its elevation angle could be changed.
2. The radar sensor could be placed slightly higher above the ground.
3. The maximum detectable range can be reduced.

The intuition behind these steps, is to prevent the elevation beam width of the antennas on the radar sensor from affecting our data. We incorporate these measures, and proceed for a third round of data collection

7.2.3 Dataset - III

For this round of data collection, we choose an outdoor environment which is relatively clear of reflective metallic objects as shown in figure 7.8. The maximum range is limited 3m. The configuration parameters are given in table 7.3. In this dataset, we use one transmitter - four receiver configuration. The data will be extracted for each of these four antennas and visualised. The range profile of a metallic reflector plate held by an individual placed 2m in front of the radar, moving with a zero velocity is shown in figure 7.9 while the range-doppler profile is shown in figure 7.10. The sensor generates one frame per second at this point.

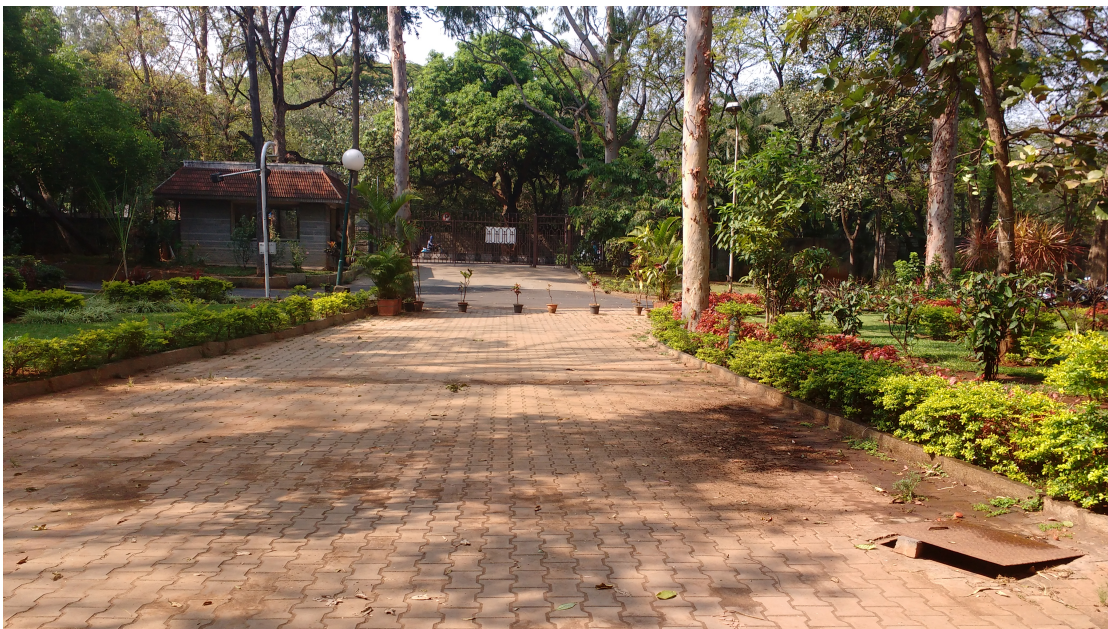


Figure 7.8: A view of the environment for the second round of data collection

PARAMETER	VALUE
Start Frequency	77GHz
Frequency Slope	100MHz/ μ s
Idle Time	739 μ s
Tx start time	0 μ s
ADC start time	7 μ s
ADC samples	64
Sample rate	2MHz
Chirp Time	40 μ s
Rx antenna gain	30dB
No. of chirps	32
Sensor orientation	0°

Table 7.3: Configuration parameters for round-3 of data collection

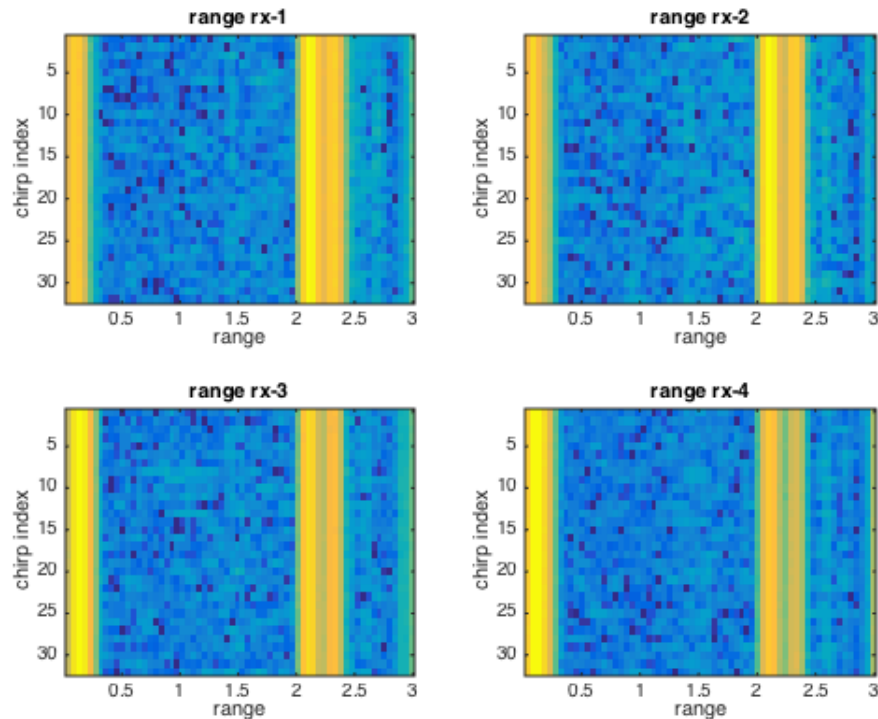


Figure 7.9: Range profile for the target kept at 2m

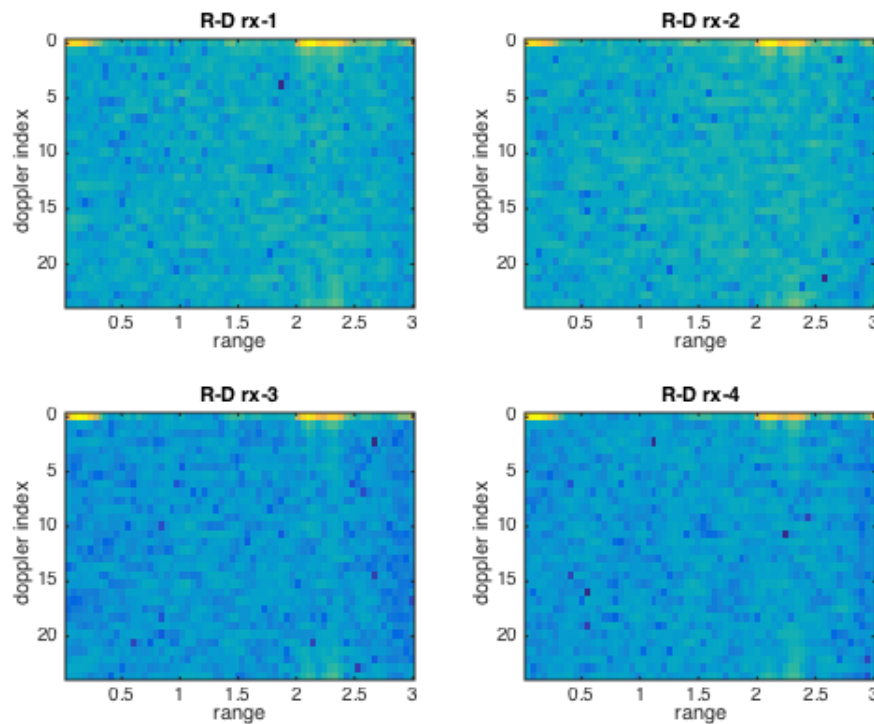


Figure 7.10: Range-doppler profile for the target kept at 2m

In figure 7.9, the target appears to have some girth. This is due to the individual holding the metallic reflector. However, the strong reflection comes off the metallic reflector which is exactly at 2m. The range doppler profile of the same object is presented in figure 7.10, and shows the velocity of all objects to be zero. In both of these figures, one notices a strong set of peaks near the origin. This is due to the self-coupling that takes place between the transmitter and receiver antennas of the radar. Having obtained this data, we now try a set of experiments to study the micro-doppler effect. Specifically, we conduct the following experiments.

1. A metallic reflector is kept static in front of the radar at 2m, and its micro-doppler profile is studied by applying a time-frequency distribution.
2. The above experiment is repeated with the metallic reflector being moved to and fro.
3. A table fan is placed at 2m, and is turned on. The micro-doppler profile of this fan is studied.

All the data samples in this dataset have 32 chirps per frame, implying we have 32 doppler or velocity bins. Thus, we use the Pseudo-Wigner Ville distribution (PWVD) as our time-frequency distribution for analysis. A Short Term Fourier Transform (STFT) will not work well here, due to its poor resolution and lesser number of samples in the data. Figure 7.11 shows the micro-doppler signatures for the three cases. We observe that these experimental results conform to the theory discussed in chapter 6. The static case produces

no doppler and is perfectly centred about the zero frequency. The moving reflector case shows some variation about the zero doppler line while the fan signature resembles a sinusoid. Improved signatures can be seen when more time samples are available, or rate at which the sensor transmits the frames increases.

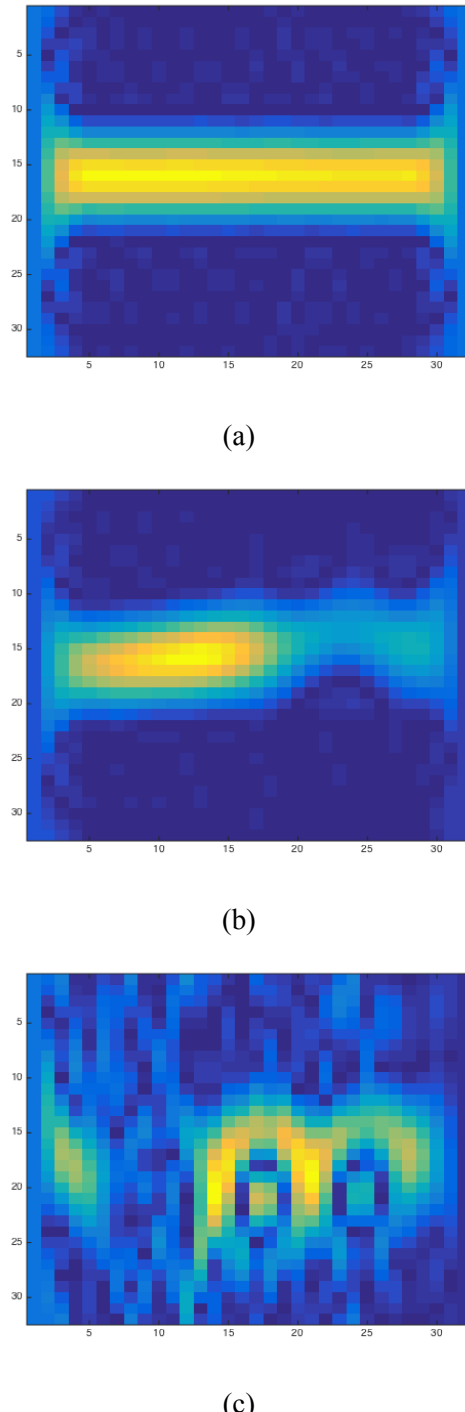


Figure 7.11: Micro-doppler profile for different objects (a) shows the profile of a static reflector (b) shows the profile of a moving reflector (c) shows the profile of a table fan. X-axis represents time and Y-axis represents the frequency. Bin 16 corresponds to the zero doppler frequency

It is clear that for a better micro-doppler signature, we need larger number of chirps. We

PARAMETER	VALUE
Start Frequency	77GHz
Frequency Slope	$27.412\text{MHz}/\mu\text{s}$
Idle Time	$3888\mu\text{s}$
Tx start time	$1\mu\text{s}$
ADC start time	$7\mu\text{s}$
ADC samples	64
Sample rate	2MHz
Chirp Time	$18.24\mu\text{s}$
Rx antenna gain	30dB
No. of chirps	128
Sensor orientation	0°

Table 7.4: Configuration parameters for round-4 of data collection

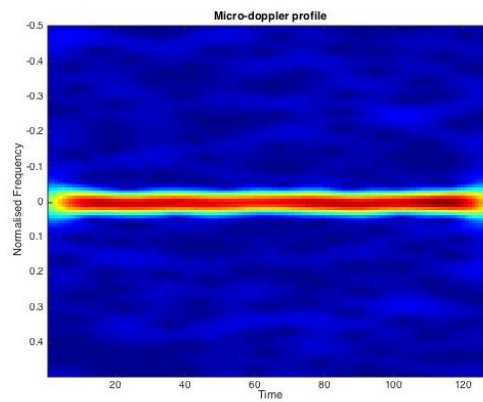
modify the configuration file to transmit a larger number of chirps.

7.2.4 Dataset - IV

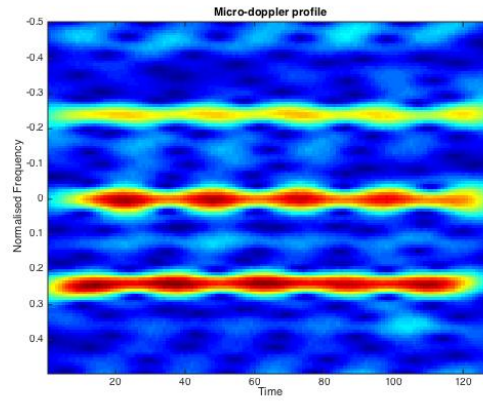
This data is collected in the same environment as before. The only difference being that we transmit 128 chirps instead of 32. The configuration parameters are listed in table 7.4. There is a small problem, in that this configuration generates more than 64kB of data. Therefore, we cannot extract all the range bins. We can extract only 16 of these range bins. The focus here however, is to study the micro-doppler profile which is why we oblige to having to make this tradeoff. We illustrate a sample result from this round of data collection wherein the micro-doppler profile of a table fan as viewed from the front is obtained when the fan is off, versus when it is on. The visualised data is shown in figure 7.12

It can be seen from the figure, that there is a marked difference between profile for a static case and the rotating case. The line along the zero-doppler frequency is the pivot on which the blades of the fan are mounted.

In all these datasets collected so far, the data was being produced at one frame per second by the board. This can be an impediment when we need continuously monitor an environment, without significant break between two observation intervals. Changing this frame rate does not alter the characteristic of the chirp. Therefore, the same configuration parameters can be used. The only precaution we need to take is to reduce the number of range bins further, from 16 to 4 since the memory is overwritten four times as faster as before.



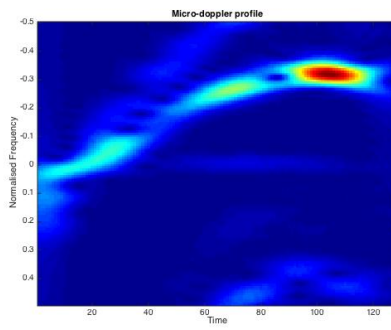
(a)



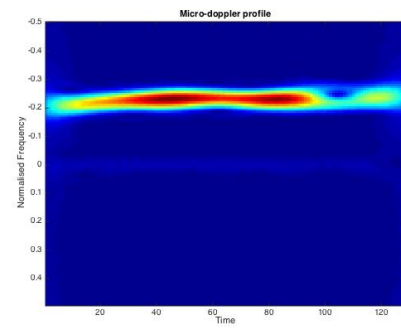
(b)

Figure 7.12: The micro-doppler for a (a) static (b) rotating table fan when viewed from the front

We visualise data obtained from a rotating reflector, and compare it against one with translational velocity. One can see the sinusoidal behaviour, in case of the rotating reflector while the doppler frequency produced by the body with translational motion stays constant, indicating nearly uniform velocity.



(a)



(b)

Figure 7.13: Micro-doppler signature for reflector with (a) rotational velocity (b) translational velocity. Notice the sinusoidal behaviour for the rotational case

In this section, we looked at the various scenarios under which data collection took place.

In the next section, we introduce feature extraction schemes to mathematically distinguish between rotating and non-rotating objects. We will use the data captured using 128 chirps, as the micro-doppler signature contains more time samples than in the case of 32 chirps.

7.3 Feature Extraction

In the previous section, we visualised a few datasets and observed the behaviour of the micro-doppler spectrum for static objects, objects with translational motion having nearly constant velocity and objects with rotational motion. We now need to arrive at some scheme, to distinguish between such objects mathematically. The output of such a scheme is called a feature, and is used to train suitable classifiers to help us distinguish targets based on their micro-doppler signature. We investigate two approaches to extracting features. The first approach proposed by Molchanov [23] uses frequency correlation, while the second approach by Zabalza et al. [24] uses Principal Component Analysis (PCA) [17]. We begin our discussion with Molchanov's approach.

7.3.1 Correlation Method

This technique consists of ideas borrowed from Molchanov [23]. In this technique, we begin by finding the correlation between frequency components appearing in the micro-doppler spectrum, across time. The idea here, is that the micro-doppler spectrum consists of the bases which need to be extracted to obtain classification features. Let us assume the micro-doppler time-frequency distribution is given by $X(f, t)$. The correlation matrix is calculated as

$$\zeta(f_1, f_2) = \sum_{t=1}^{T_f} X(f_1, t)X(f_2, t) \quad (7.1)$$

where the summation is over the frame time. This is expected to be a symmetric matrix, which means $\zeta(f_1, f_2) = \zeta(f_2, f_1)$. The next step, is to estimate the eigenpairs for this $\{\psi_r, \lambda_r\}$ where, ψ_r is the r^{th} eigenvector, and λ_r is the corresponding eigenvalue. These eigenpairs can be obtained upon Eigen decomposition of the correlation matrix ζ .

Now, we take the Fourier Transform of the eigenvectors. This is done to obtain features where most of the signal information is concentrated. We notice that the information is contained in the low frequency components, which is why it is sufficient to compute only the first k fourier coefficients, where k can be chosen based on requirement. This can be mathematically represented as

$$y_r = \bigcup_{l=1}^k \left\{ \left| \sum_{f=1}^M \psi_r(f) e^{\frac{-j2\pi fl}{M}} \right| \right\} \quad (7.2)$$

We now obtain the feature vector F , by considering the eigen vector which corresponds to

the largest eigen value. This approach is somewhat related to Principal Component Analysis [17], with the difference being that the data is not mean centred. In our case, the eigen vector corresponding to the largest eigenvalue is the mean vector.

We now understand the above steps through three examples, one each of the static, translational and rotational case. The visualisation at the end of each stage is shown for a rotating target in figure 7.14. If we notice a visualisation of the correlation matrix given in figure 7.14b, we can observe the symmetry, and the fact that the matrix is sparsely populated. The Fourier Transform of the eigen vector corresponding to the largest eigen value is shown in figure 7.14c. From this, the fact that only initial few coefficients contain information, is evident. In practise, we consider only the first thirty coefficients while building our feature vector.

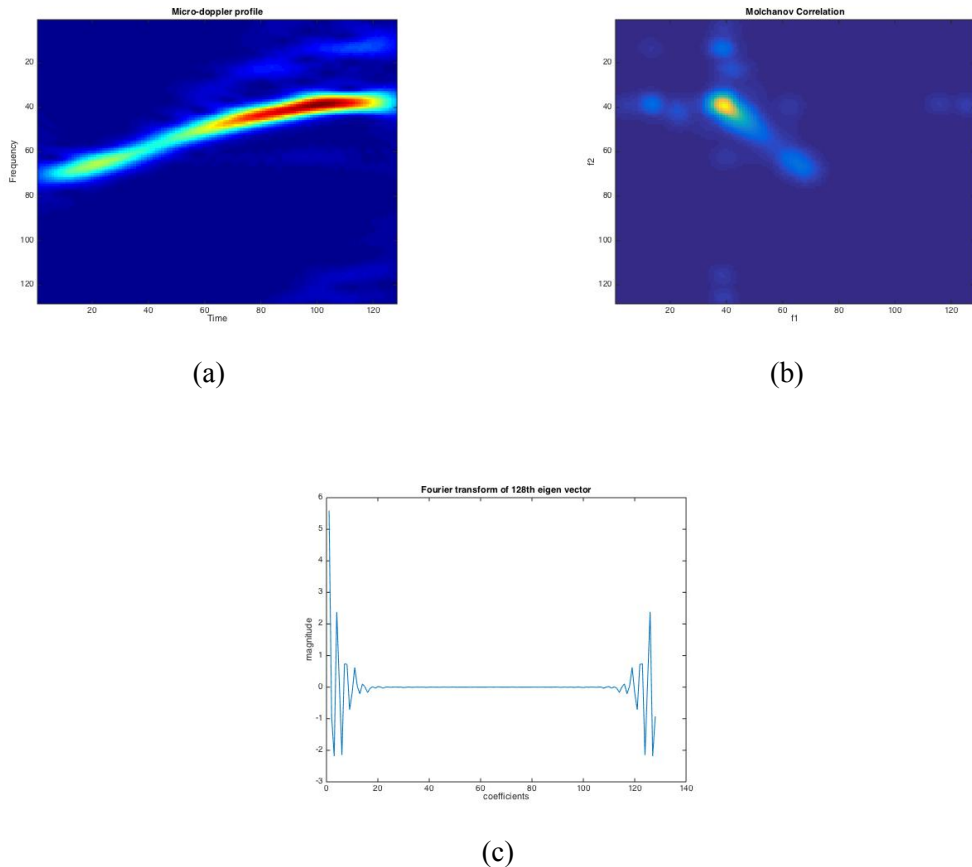


Figure 7.14: Steps in correlation method, (a) Shows the micro-doppler spectrum (b) Visualisation of the correlation matrix (c) The Fourier Transform of the eigenvector with largest eigenvalue. Notice the symmetry of the correlation matrix in (b), and the fact that only the first few coefficients in (c) contain information

We plot the same set of figures for a target moving with uniform linear velocity in figure 7.15. One can notice a difference in the appearance of the correlation matrix and the transformed eigenvector. We conclude our discussion on correlation method, by visualising the output of various steps for a stationary target, plotted in figure 7.16.

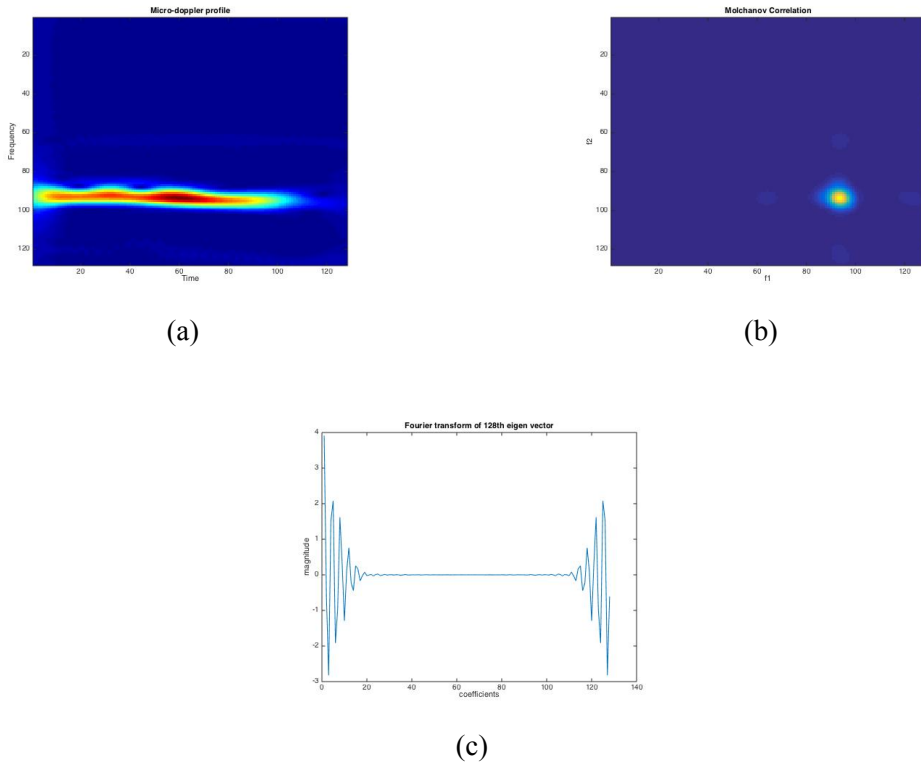


Figure 7.15: Steps in correlation method, (a) Shows the micro-doppler spectrum (b) Visualisation of the correlation matrix (c) The Fourier Transform of the eigenvector

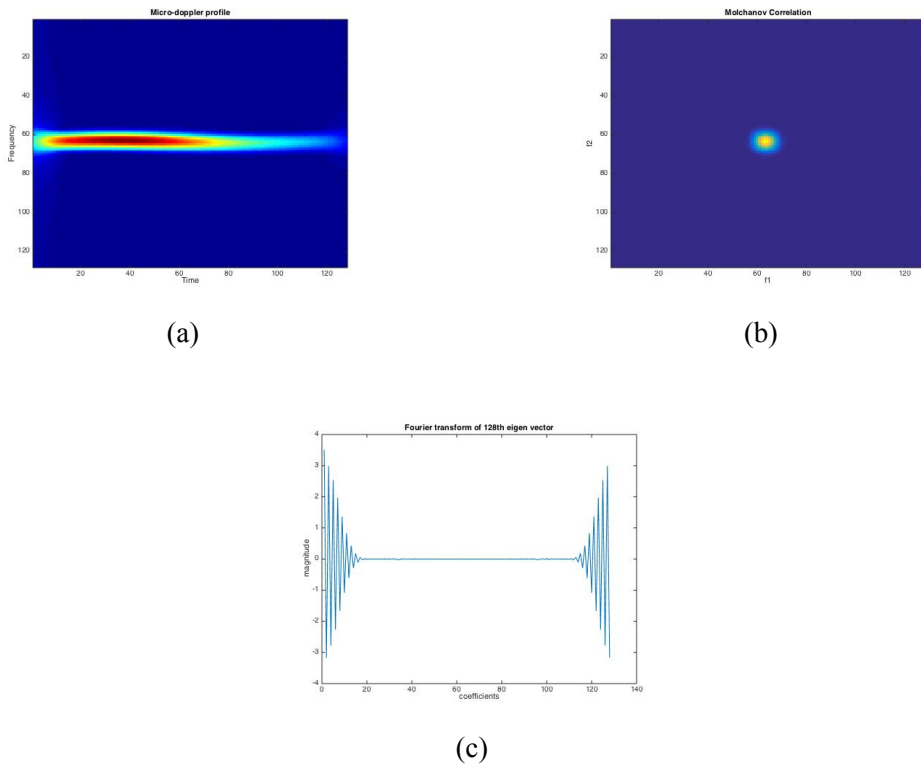


Figure 7.16: Steps in correlation method, (a) Shows the micro-doppler spectrum (b) Visualisation of the correlation matrix (c) The Fourier Transform of the eigenvector

7.3.2 Principal Component Analysis Method

This method consists of ideas borrowed from Zabalza et al. [24]. As in the correlation method, we begin by obtaining the micro-doppler spectrum $X(f, t)$. From this information, we calculate the Mean Frequency Profile Λ given by

$$\Lambda(f) = \frac{1}{T} \sum_{t=1}^T |x(f, t)| \quad (7.3)$$

where T is the number of time instants or columns in the micro-doppler spectrum. The MFP for objects with different motion types is depicted in figure 7.18. One might argue that this is equal to taking the Fourier Transform over a single range bin, as discussed in Algorithm 1 in Chapter 4. However, this is not the case. The reason is a bit mathematically involved, and is explained in Cohen's textbook [14]. The slight difference between the two is illustrated in figure 7.17. The MFP represents two main features. The location of the principal peak represents the velocity that appear when a body moves, while the spread in peaks and the width of each peak represents the variation in the velocity during the interval of observation.

We now reduce the dimensionality of this data using Principal Component Analysis (PCA) [17]. The MFP is a 128 dimensional vector, and we attempt to reduce this to 30 dimensions. The objective now, is to find a transformation matrix that helps us achieve this reduction. We begin by stacking the MFP vectors of each training sample into a matrix. The covariance matrix of this data is found, and subjected to a Singular Value Decomposition (SVD). The vectors corresponding to the top 30 singular values are chosen to constitute the transformation matrix. Multiplying this matrix with the training or test data vector helps reduce the dimensionality of the data.

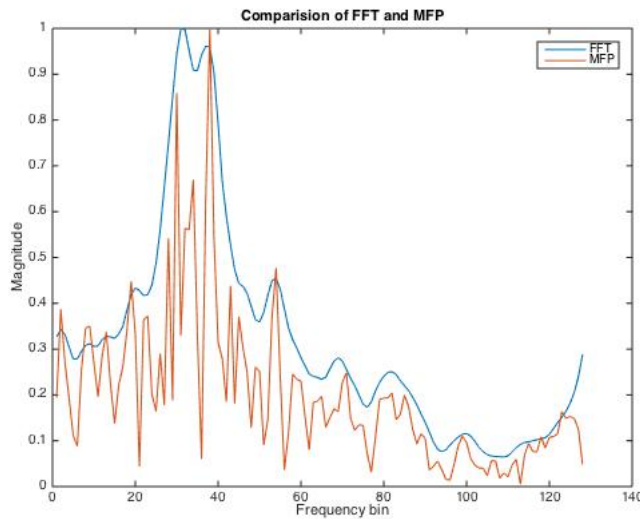


Figure 7.17: Fourier Transform v/s Mean Frequency Profile

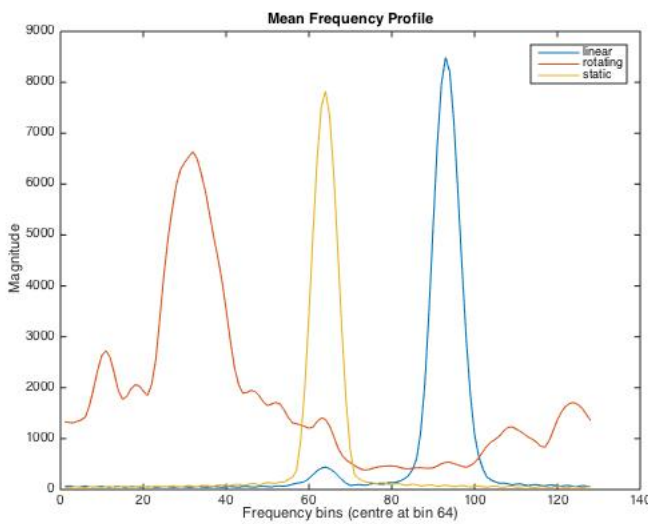


Figure 7.18: Mean Frequency Profile for different kinds of motion

7.4 Classification

In the last section, we understood two methodologies to extract features from the micro-doppler data. Now, we formulate a binary classification problem which can be stated as follows

Given the micro-doppler spectrum of a target, identify whether this target is rotating or not.

We investigate the performance of the following classifiers in helping us fulfil this objective

1. Naïve Bayes'
2. Support Vector Machines (linear, polynomial and Gaussian rbf)
3. K-Nearest Neighbours with $k = 1, 2, 3, 4$

We examine the performance of these classifiers using features extracted from both the above methods [15, 16].

7.4.1 Classification Using the Correlation Method

In this section we present the classification results with features extracted using the correlation method. Out of all available data samples, 70% of the data is used for training and 30% is used for testing. The performance of the classifiers are represented using confusion matrices, and the overall accuracy of classification. Upon studying the results from the tables below, one can see that Naïve Bayes, linear and polynomial SVMs and KNN classifiers give similar results. If the dimensionality of the data changes, the performance of the Naïve

Bayes classifier is known to degrade sharply, which is why we would prefer to use either an SVM or a KNN classifier. The SVM using a Gaussian kernel shows poor performance when tested with data from non-rotating objects. This problem arises due to overfitting of data by the SVM, and is thus not used.

Naïve Bayes		
Class	Rotating	Non-rotating
Rotating	96.33%	3.60%
Non-rotating	33.80%	66.17%

Table 7.5: Confusion matrix for the Naïve Bayes classifier using the correlation method for feature extraction

Support Vector Machine						
	Linear		Polynomial		Gaussian rbf	
Class	Rotating	Non-rotating	Rotating	Non-rotating	Rotating	Non-rotating
Rotating	90.82%	9.17%	92%	8%	100%	0%
Non-rotating	26.47%	73.52%	20.58%	79.41%	55.88%	44.11%

Table 7.6: Confusion matrix for the SVM classifier using the correlation method for feature extraction

K-Nearest Neighbours									
	K=1		K=2		K=3		K=4		
Class	Rotating	Non-rotating	Rotating	Non-rotating	Rotating	Non-rotating	Rotating	Non-rotating	
Rotating	88.07%	11.92%	80.73%	19.26%	90.82%	9.17%	88.99%	11%	
Non-rotating	17.64%	82.35%	5.88%	94.11%	17.64%	82.35%	14.70%	85.29%	

Table 7.7: Confusion matrix for the KNN classifier using the correlation method for feature extraction

Naïve Bayes	Support Vector Machine			K-Nearest Neighbours			
	Linear	Polynomial	Gaussian rbf	K=1	K=2	K=3	K=4
84.70%	84.10%	87%	78.53%	85.87%	86%	87.57%	87.57%

Table 7.8: Overall accuracy for the classifiers using the correlation method for feature extraction

7.4.2 Classification Using the PCA Method

Now, we evaluate the performance of the classifiers trained and tested with features extracted using the PCA method. As in the previous section, 70% of available data is used

to train while 30% is used to test, with confusion matrices and the overall accuracy used as metrics to evaluate the performance. If we examine these results given below, it is quite clear that the SVM and KNN classifiers outperform the Naïve Bayes classifier. The trend here is similar to the one obtained in the previous subsection, validating our proposition to use either an SVM or a KNN classifier in practise.

Naïve Bayes		
Class	Rotating	Non-rotating
Rotating	87.15%	12.80%
Non-rotating	39.70%	60.29%

Table 7.9: Confusion matrix for the Naïve Bayes classifier using the PCA method for feature extraction

Support Vector Machine						
	Linear		Polynomial		Gaussian rbf	
Class	Rotating	Non-rotating	Rotating	Non-rotating	Rotating	Non-rotating
Rotating	92.66%	7.33%	88%	12%	100%	0%
Non-rotating	11.76%	88.23%	12.67%	87.32%	55.88%	44.11%

Table 7.10: Confusion matrix for the SVM classifier using the PCA method for feature extraction

K-Nearest Neighbours									
	K=1		K=2		K=3		K=4		
Class	Rotating	Non-rotating	Rotating	Non-rotating	Rotating	Non-rotating	Rotating	Non-rotating	
Rotating	88.07%	11.92%	80.73%	19.26%	88.99%	11.00%	81.65%	18.34%	
Non-rotating	5.88%	94.11%	4.41%	95.58%	14.70%	85.29%	8.82%	91.17%	

Table 7.11: Confusion matrix for the KNN classifier using PCA method for feature extraction

Naive Bayes	Support Vector Machine			K-Nearest Neighbours			
	Linear	Polynomial	Gaussian rbf	K=1	K=2	K=3	K=4
76.83%	90.96%	88%	78.50%	90.39%	86%	87.57%	85.31%

Table 7.12: Overall accuracy of classifiers using the PCA method for feature extraction

Whether to choose SVM or KNN, depends on the type of classification problem to be solved. The KNN algorithm naturally adapts to problems with more number of classes.

In our case, a problem with multiple classes could be to classify between UAV's, birds and helicopters. SVMs on the other hand, break down this multi-class problem into a one-against-one or a one-against all problem, i.e., reduces it into smaller binary classification problems and then goes about performing classification. However, since the training phase of an SVM involves solving an optimisation problem, it is bound to give us the optimal solution. The SVM is also newer, and closer to the state of the art compared to the KNN classifier.

Thus, we have accomplished our primary aim of being able to distinguish rotating from non-rotating targets using two methods of feature extraction. The performance can be improved by combining multiple classifiers, using the concept of *boosting*. This takes the maximum value across the predictions made by classifiers and declares that to be the predicted value.

Chapter 8

Conclusion and Future Work

The objective of this project was to develop a scheme to classify targets within the field of view of a radar. This problem was simplified, to first differentiate the rotating targets from the non-rotating targets. An FMCW radar sensor operating at 77 GHz was deemed suitable for this application owing to its fine range and velocity resolutions. Specifically, the AWR1642 sensor developed by Texas Instruments was chosen. The radar signal processing pipeline for an FMCW radar was studied, and implemented to localize a target with its range and velocity. Two simulation models, for simple and unevenly shaped targets were developed and their performance was studied. Obtaining the micro-doppler spectrum of a target was identified as the first step to better understand the nature of the motion of a target. Time-frequency analysis was used to evaluate the micro-doppler spectrum of a target. Two feature extraction schemes were discussed to extract features differentiating the rotating targets from the non-rotating targets. Finally, the performance of classifiers was studied using the features extracted from these two techniques, thereby solving our simplified binary classification problem.

There is a significant amount of work to be done to meet the larger objective of the project. There is a need to develop more detailed and realistic simulation models to understand the behavior of various types of targets, environments and algorithms. There is a need to understand the full range of capabilities and functionality provided by the AWR1642 sensor. In the area of classification, there is a need to improve upon existing feature extraction schemes, identify scaling invariant features, and also develop robust signal processing algorithms. That is, the feature size must be independent of the dimensions of the micro-doppler spectrum. This way, our classification scheme is independent of the configuration used by the board to obtain data, which includes different number of chirps, bandwidth etc. The binary classification problem must be scaled to incorporate more classes, which would enable to distinguish between different rotating objects.

Appendix A

Doppler Effect

Doppler effect is the change in frequency of a sound or electromagnetic wave due to relative motion between the source and the observer. In our case, the target reflecting the waves is the source, and the radar is the observer. We now understand the relationship between the velocity of a target, and the corresponding change in frequency, known as the doppler frequency.

Consider a stationary radar, and a moving target separated by a distance R at a given instance of time, as shown in figure A.1. The target moves with a velocity v_r relative to the radar along the line of sight.

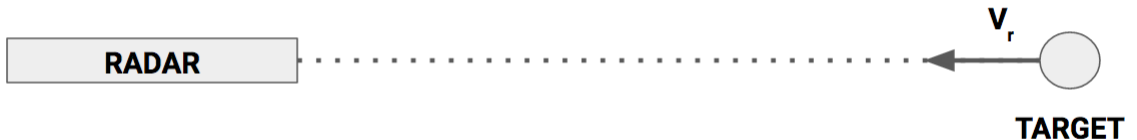


Figure A.1: Diagram to derive relationship between target velocity and doppler frequency

Assume the transmitted signal has a frequency of f_0 . A transmitted wave moves from the radar, gets reflected off the target and returns to the radar. Assuming this delay is negligible compared to the time required to cause a significant change in velocity, the distance travelled by the wave is $2R$, and thus the number of wavelengths traversed in such a case is

$$n = \frac{2R}{\lambda} \quad (\text{A.1})$$

The total phase excursion is then

$$\phi = \frac{2R}{\lambda} 2\pi \quad (\text{A.2})$$

It is evident that when a target moves, R as well as ϕ changes, which implies that we now

have an angular frequency associated with this movement given by

$$\frac{d\phi}{dt} = \frac{4\pi}{\lambda} \frac{dR}{dt} \quad (\text{A.3})$$

dR/dt is nothing but the velocity of the target, given by v_r . We can also equate the above equation to $W_d = 2\pi f_d$, where f_d is the doppler frequency. Combining these terms together, gives us

$$f_d = \frac{2v_r}{\lambda} \quad (\text{A.4})$$

which is the relationship between the velocity of the target, and the frequency shift produced in the received signal, or the doppler frequency. If the target is moving in a direction other than along the line of sight as shown in figure A.2, we consider the component of velocity along the radial direction to calculate the doppler frequency.



Figure A.2: Diagram to derive doppler frequency for object not moving along line of sight

In figure A.2, the velocity component along the line of sight is $vcos(\theta)$. Therefore, equation A.4 becomes

$$f_d = \frac{2vcos(\theta)}{\lambda} \quad (\text{A.5})$$

The point to note, is that the doppler frequency is a function of the target velocity along the line of sight alone. The sign of the doppler frequency is negative for targets moving towards the radar, and positive for objects moving away from the radar.

Appendix B

Time-Frequency Distributions

We now review some of time-frequency distributions that can be used to obtain the micro-doppler signature. In particular, we review the Short Term Fourier Transform (STFT), Wigner-Ville distribution (WVD), and the Pseudo-Wigner-Ville Distribution (PWVD). Deeper insight into the concept of time frequency analysis, and other transforms can be obtained by referring to the book by Cohen [14]. For the purpose of illustration, we use a signal containing three frequency sweeps: 150Hz - 400Hz, 650Hz - 900Hz, 2200Hz - 1600Hz.

B.1 Short Term Fourier Transform (STFT)

The transform is given by the equation

$$S(t, \omega) = \frac{1}{\sqrt{2\pi}} \int s(\tau) h(\tau - t) e^{-j\omega\tau} d\tau \quad (\text{B.1})$$

where $s(\tau)$ is the signal to be analyzed, $h(\tau)$ is a window function, which helps us achieve time localisation. The window function helps in achieving this, by suppressing the signal content outside of it. The energy density spectrum, is given by

$$P(t, \omega) = |S(t, \omega)|^2 = \left| \frac{1}{\sqrt{2\pi}} \int s(\tau) h(\tau - t) e^{-j\omega\tau} d\tau \right|^2 \quad (\text{B.2})$$

and is commonly referred to as the spectrogram. The result of applying STFT to the signals described before, is given in figure B.1. One can see, that the resolution of the plot along the frequency axis is poor, and the frequency band is not as fine as expected. The poor resolution is one of the main disadvantages of the STFT, and is a consequence of the uncertainty principle in signal processing.

The need now is to find a transform which provides better resolutions in time and frequency, and one such transform is the Wigner-Ville Distribution (WVD)

B.2 Wigner-Ville Distribution (WVD)

The WVD for a signal $s(t)$ is given by

$$W(t, \omega) = \frac{1}{2\pi} \int s^* \left(t - \frac{\tau}{2} \right) s \left(t + \frac{\tau}{2} \right) e^{-j\omega\tau} d\tau \quad (\text{B.3})$$

What this equation does, is find the Fourier Transform of the local autocorrelation of the signal. This helps us achieve the time localisation. The Wigner-Ville distribution for the test signal is shown in figure B.2. It can be observed that the three frequency sweeps appear much finer than before, but at the cost of interference in the spectrum. This interference occurs due to the cross correlation terms appearing when taking the local correlation. Another factor for the interference to appear, is that the localisation is not as good as in STFT. The key advantage here however, is the better resolution. The interference is reduced upon using the Pseudo-Wigner Ville distribution (PWVD).

B.3 Pseudo-Wigner Ville Distribution (PWVD)

The PWVD of a signal $s(t)$ is given by

$$W_p(t, \omega) = \frac{1}{2\pi} \int h(\tau) s^* \left(t - \frac{\tau}{2} \right) s \left(t + \frac{\tau}{2} \right) e^{-j\omega\tau} d\tau \quad (\text{B.4})$$

Where $h(\tau)$ is a window function to improve localisation of the signal. This window function causes a slight deterioration in the resolution, as the energy characteristics of the window functions are now superimposed over that of the original signal. The result of applying PWVD to the test signal is shown in figure B.3. It can be seen that we get finer resolutions than the STFT, with reduced interference compared to the Wigner-Ville Distribution.

We now perform a simple experiment, where we attempt to obtain a spectrum with the fine resolution of the WVD without the interference, as in an STFT. This is achieved by using the STFT as a mask over the WVD and extracting only those frequencies truly existing in the signal. The result of this experiment is shown in fig B.4. The output does meet the requirements, but at the cost of computational efficiency. Introducing this algorithm into a larger processing pipeline could increase the computation delay.

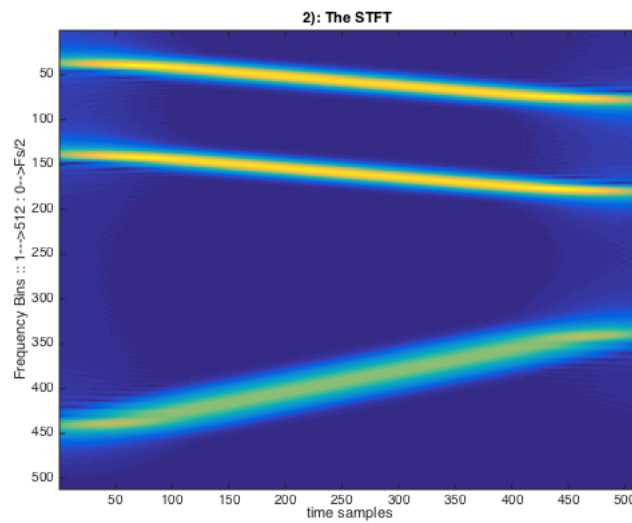


Figure B.1: STFT for the test signal

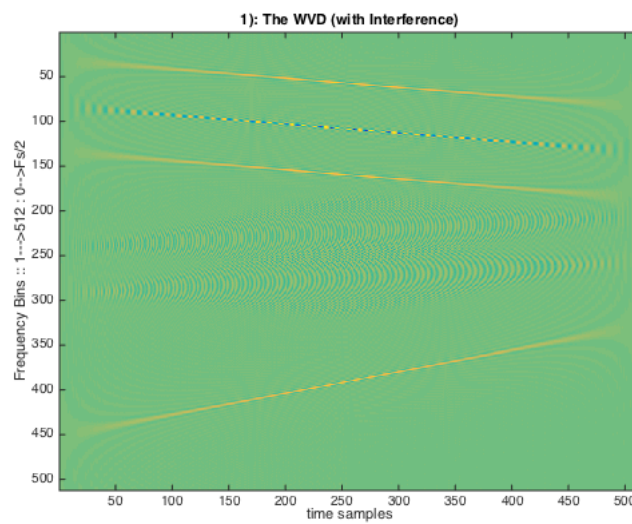


Figure B.2: WVD for the test signal

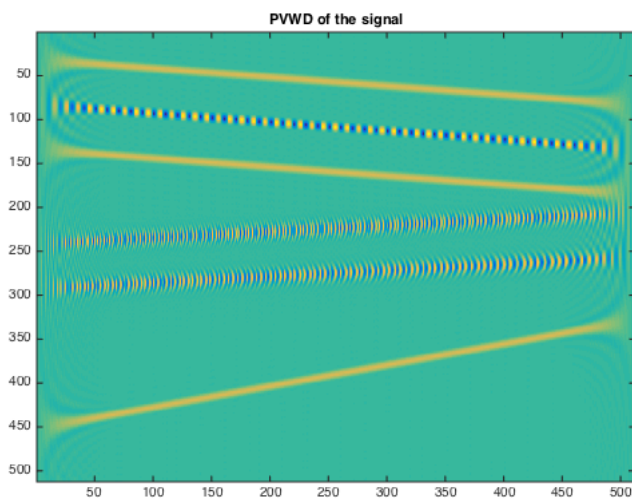


Figure B.3: PWVD for the test signal

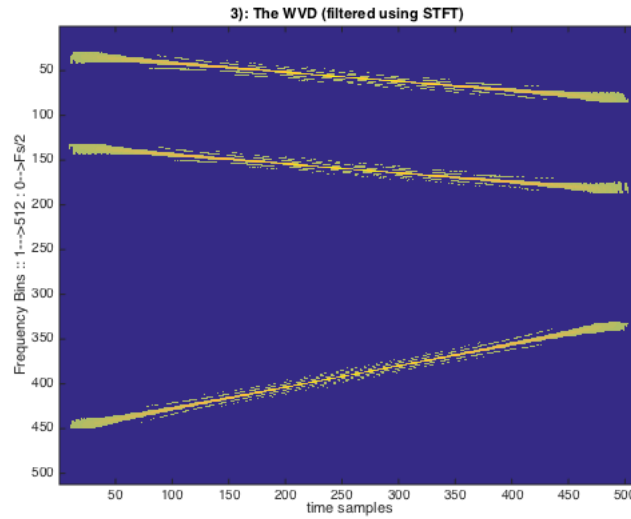


Figure B.4: WVD masked with STFT

The usage of a particular transform is application specific and varies from one set of data to another. For example, when there is a lack of time samples in the data, taking a WVD or PWVD is a better alternative as compared to an STFT. This is of course, at the cost of interference terms being added to the spectrum.

Bibliography

- [1] T. K. Sarkar, M. S. Palma, and E. L. Mokole, “Echoing across the years: A history of early radar evolution,” *IEEE Microwave Magazine*, vol. 17, no. 10, pp. 46–60, 2016.
- [2] K. Ahsan, H. Shah, and P. Kingston, “RFID applications: An introductory and exploratory study,” *CoRR*, vol. abs/1002.1179, 2010. [Online]. Available: <http://arxiv.org/abs/1002.1179>
- [3] G. Reina, D. Johnson, and J. P. Underwood, “Radar sensing for intelligent vehicles in urban environments,” in *Sensors*, 2015.
- [4] J. Lien, N. Gillian, M. Karagozler, P. Amihood, C. Schwesig, E. Olson, H. Raja, and I. Poupyrev, “Soli: Ubiquitous gesture sensing using millimeter wave radar,” in *ACM Trans. Graph. 35*, Jul 2016, p. 19.
- [5] S. Aigerim, A. Askhat, and A. Yedilkhan, “Recognition of 3d object using kinect,” in *2015 9th International Conference on Application of Information and Communication Technologies (AICT)*, 2015, pp. 341–346.
- [6] B. Chen, Z. Huang, W. Yu, Y. Xu, and J. Peng, “Object recognition and localization based on kinect camera in complex environment,” in *2013 IEEE International Conference on Robotics and Biomimetics (ROBIO)*, 2013, pp. 668–673.
- [7] *AWR1642 Single-chip 77 and 79 GHz FMCW Radar Sensor*, Texas Instruments, 5 2017.
- [8] C. Balanis, *Antenna Theory: Analysis and Design*, 2nd ed., 1996.
- [9] M. I. Skolnik, *Introduction to Radar Systems*, 2nd ed. McGraw-Hill College, 1980.
- [10] D. Ghose. Chapter 3: Continuous wave and frequency modulated radar. [Online]. Available: <http://nptel.ac.in/courses/101108056/module2/lecture4.pdf>
- [11] D. E. Barrick, “Fm/cw signals and digital processing,” NOAA Tech.Report.ERL 283-WPL, Tech. Rep., 1973.
- [12] S. Rao. Introduction to mm-wave sensing. [Online]. Available: <https://training.ti.com/intro-mmwave-sensing-fmcw-radars-module-1-range-estimation>

- [13] P. Suresh, T. Thayaparan, T. Obulesu, and K. Venkataramaniah, “Extracting micro-doppler radar signatures from rotating targets using fourier bessel transform and time frequency analysis,” *IEEE Transactions on Geoscience and Remote Sensing*, vol. 52, no. 6, pp. 3204–3210, June 2014.
- [14] L. Cohen, *Time-frequency analysis: Theory and Applications*. Prentice Hall, Inc, 1995.
- [15] D. G. S. Richard O. Duda, Peter E. Hart, *Pattern classification*, 2nd ed. Wiley, 2001.
- [16] C. M. Bishop, *Pattern Recognition and Machine Learning*, 1st ed., ser. Information science and statistics. Springer, 2006.
- [17] J. Shlens, “A tutorial on principal component analysis,” *CoRR*, vol. abs/1404.1100, 2014.
- [18] *MMWAVE SDK User Guide*, Texas Instruments, 10 2017.
- [19] K. Ramasubramanian, *Using a complex-baseband architecture in FMCW radar systems*, Texas Instruments, 10 2017.
- [20] T. Wei and X. Zhang, “mtrack: High-precision passive tracking using millimeter wave radios,” in *Proceedings of the 21st Annual International Conference on Mobile Computing and Networking*, ser. MobiCom ’15. ACM, 2015, pp. 117–129.
- [21] V. C. Chen, *The Micro-Doppler Effect in Radar (Artech House Radar Library)*. Artech House Publishers, 2011.
- [22] S. Rahman and D. Robertson, “Time-frequency analysis of millimeter-wave radar micro-doppler data from small uavs,” in *2017 Sensor Signal Processing for Defence Conference (SSPD)*, 2017, pp. 1–5.
- [23] P. Molchanov, “Radar target classification by micro - doppler contribution,” Ph.D. dissertation, Tampere University of Technology, 2014.
- [24] J. Zabalza, G. D. C. C. Clemente, J. S. J. Ren, and S. Marshall, “Robust pca micro-doppler classification using svm on embedded systems,” *IEEE Transactions on Aerospace and Electronic Systems*, vol. 50, no. 3, pp. 2304–2310, July 2014.
- [25] J. J. M. de Wit, P. van Dorp, and A. G. Huizing, “Classification of air targets based on range-doppler diagrams,” in *2016 European Radar Conference (EuRAD)*, Oct 2016, pp. 89–92.